



OPEN

RNF43 mutations predict response to anti-BRAF/EGFR combinatory therapies in BRAF^{V600E} metastatic colorectal cancer

Elena Elez^{1,2}✉, Javier Ros^{1,2,3}, Jose Fernández², Guillermo Villacampa², Ana Belén Moreno-Cárdenas², Carlota Arenillas^{2,4}, Kinga Bernatowicz^{1,2}, Raquel Comas², Shanshan Li⁵, David Philip Kodack⁶, Roberta Fasani², Ariadna Garcia², Javier Gonzalo-Ruiz^{1,2}, Alejandro Piris-Gimenez², Paolo Nuciforo^{1,2}, Grainne Kerr⁷, Rossana Intini⁸, Aldo Montagna⁸, Marco Maria Germani⁹, Giovanni Randon¹⁰, Ana Vivancos², Ron Smits^{1,5}, Diana Graus^{7,13}, Raquel Perez-Lopez^{2,11}, Chiara Cremolini⁹, Sara Lonardi^{1,8}, Filippo Pietrantonio^{1,10}, Rodrigo Dienstmann², Josep Tabernero^{1,2,4,12} and Rodrigo A. Toledo^{2,4}✉

Anti-BRAF/EGFR therapy was recently approved for the treatment of metastatic BRAF^{V600E} colorectal cancer (mCRC^{BRAF-V600E}). However, a large fraction of patients do not respond, underscoring the need to identify molecular determinants of treatment response. Using whole-exome sequencing in a discovery cohort of patients with mCRC^{BRAF-V600E} treated with anti-BRAF/EGFR therapy, we found that inactivating mutations in RNF43, a negative regulator of WNT, predict improved response rates and survival outcomes in patients with microsatellite-stable (MSS) tumors. Analysis of an independent validation cohort confirmed the relevance of RNF43 mutations to predicting clinical benefit (72.7% versus 30.8%; $P = 0.03$), as well as longer progression-free survival (hazard ratio (HR), 0.30; 95% confidence interval (CI), 0.12–0.75; $P = 0.01$) and overall survival (HR, 0.26; 95% CI, 0.10–0.71; $P = 0.008$), in patients with MSS-RNF43^{mutated} versus MSS-RNF43^{wild-type} tumors. Microsatellite-unstable tumors invariably carried a wild-type-like RNF43 genotype encoding p.G659fs and presented an intermediate response profile. We found no association of RNF43 mutations with patient outcomes in a control cohort of patients with MSS-mCRC^{BRAF-V600E} tumors not exposed to anti-BRAF targeted therapies. Overall, our findings suggest a cross-talk between the MAPK and WNT pathways that may modulate the antitumor activity of anti-BRAF/EGFR therapy and uncover predictive biomarkers to optimize the clinical management of these patients.

The criteria to match patients with cancer with the most effective therapies relies on the identification of molecular tumor dependencies that can be targeted with available treatments¹. The BRAF^{V600E} mutation is found in approximately 10% of patients with metastatic colorectal cancer (mCRC), and its clinical presentation is often associated with a predominance of right-sided proximal tumors, high prevalence of microsatellite instability (MSI; near 30%), refractoriness to standard-of-care therapies and an unfavorable prognosis (Extended Data Fig. 1a)^{2,3}. Compared to mCRC^{BRAF-wild-type}, BRAF^{V600E} tumors (hereafter referred to as mCRC^{BRAF-V600E}) also associate with specific molecular features, including a low frequency of APC mutations and a high rate of mutations in the tumor suppressor gene RNF43 (refs. 4,5), a RING E3 ubiquitin ligase involved in suppression of the WNT-β-catenin pathway through promoting the degradation of FZD/WNT receptors^{6,7}.

BRAF^{V600E} ATP-competitive kinase inhibitors were designed and clinically tested for the treatment of BRAF^{V600E}-driven tumors, thus achieving variable outcomes depending on tumor type⁸. In particular, patients with melanoma harboring BRAF^{V600E} mutations have been demonstrated to derive marked benefit from BRAF inhibitor monotherapy (up to 70% objective response rate (ORR)^{9,10}), while, in stark contrast, patients with BRAF^{V600E}-mutant CRC receiving the same treatment experienced little clinical benefit^{4,8,11,12}. Preclinical studies uncovered an intricate molecular circuitry in CRC^{BRAF-V600E} leading to rapid compensatory activation of the epidermal growth factor receptor (EGFR) that likely hampered the clinical outcomes of these patients^{13,14}. These key findings set the rationale for the design of clinical trials targeting both BRAF and EGFR, with or without additional targeted therapies (that is, MEK, ERK or PIK3CA inhibitors) that generally achieved improved clinical outcomes as compared to previous standard-of-care treatments^{12,15–17}.

¹Medical Oncology Department, Vall d'Hebron University Hospital, Vall d'Hebron Barcelona Hospital Campus, Barcelona, Spain. ²Vall d'Hebron Institut de Oncologia (VHIO), Vall d'Hebron Barcelona Hospital Campus, Barcelona, Spain. ³Oncologia Medica, Dipartimento di Medicina di Precisione, Università degli Studi della Campania Luigi Vanvitelli, Naples, Italy. ⁴Centro de Investigación Biomédica en Red de Cáncer (CIBERONC), Institute of Health Carlos III (ISCIII), Madrid, Spain. ⁵Department of Gastroenterology and Hepatology, Erasmus MC-University Medical Center, Rotterdam, the Netherlands. ⁶Novartis Institutes for BioMedical Research, Cambridge, MA, USA. ⁷Oncology Department, Novartis Institutes for Biomedical Research, Novartis, Basel, Switzerland. ⁸Department of Oncology, Veneto Institute of Oncology IRCCS, Padova, Italy. ⁹Unit of Medical Oncology, Azienda Ospedaliero-Universitaria Pisana, Department of Trans-lational Research and New Technologies in Medicine, University of Pisa, Pisa, Italy. ¹⁰Department of Medical Oncology, Fondazione IRCCS Istituto Nazionale dei Tumori, Milan, Italy. ¹¹Radiology Department, Vall d'Hebron University Hospital, Vall d'Hebron Barcelona Hospital Campus, Barcelona, Spain. ¹²UVic-UCC, IOB-Quirón, Barcelona, Spain. ¹³Present address: Ridgeline Discovery, Basel, Switzerland. ✉e-mail: meelez@vhio.net; rtoledo@vhio.net

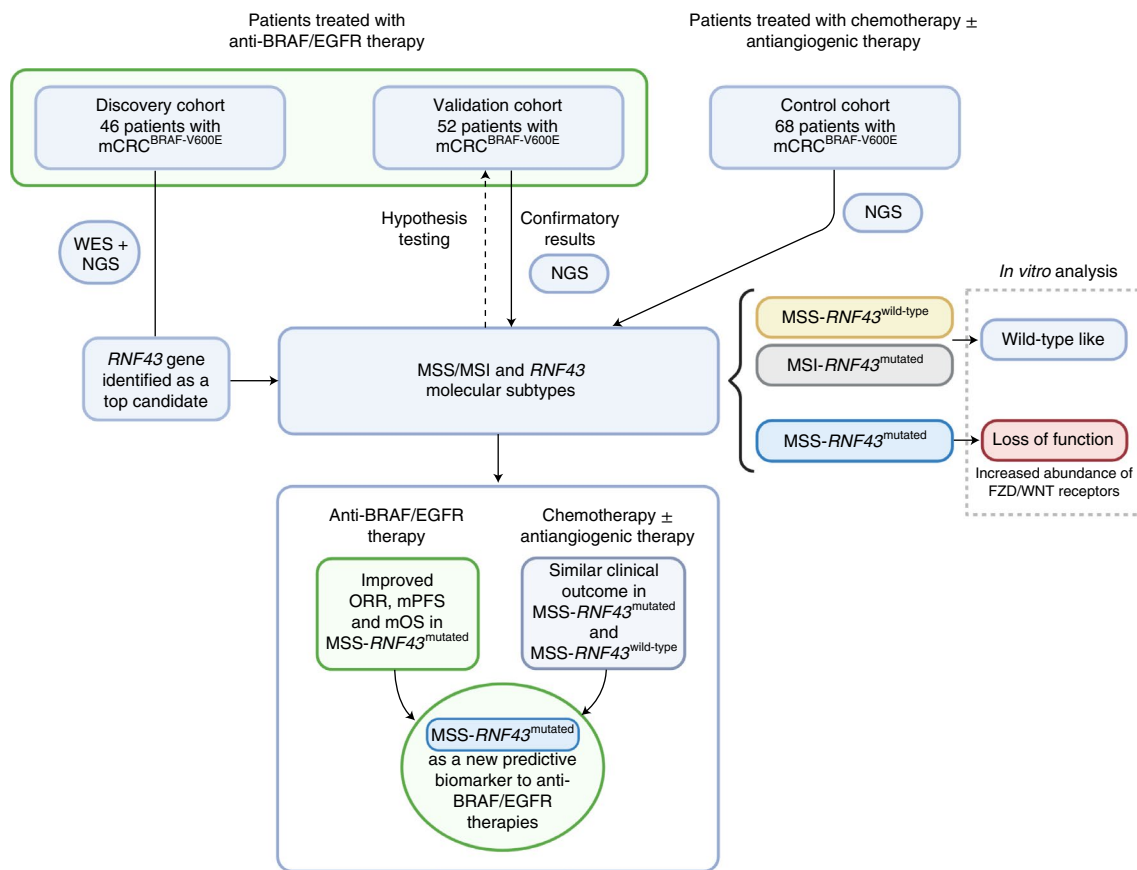


Fig. 1 | Study design. A total of 166 patients with mCRC^{BRAF-V600E} were included in the study from discovery ($n=46$), validation ($n=52$) and control ($n=68$) cohorts. WES of germline DNA, baseline tumor DNA and/or baseline plasma cfDNA from 28 patients was performed. Targeted NGS was used to assess *RNF43* tumor mutation status for the 18 remaining patients from the discovery cohort and all tumors from the validation and control cohorts. Genomic profiles and MSS/MSI-*RNF43* molecular subtypes were compared with clinical response data (ORR, mPFS and mOS) using dNdScv maximum-likelihood unbiased mutation enrichment analysis²⁵. In vitro assays were used to assess the functional impact of *RNF43* mutations detected in patient samples (see more in Fig. 6).

The clinical outcomes of patients with mCRC^{BRAF-V600E} treated with the triplet regimen of encorafenib, cetuximab and binimetinib were assessed in the phase 3 BEACON CRC trial (NCT02928224). The study showed that combinatorial blockade of BRAF and EGFR, with or without concomitant MEK inhibition, achieved improved ORR (26% with the triplet and 20% with the doublet therapy versus 2% in the control arm) and extended overall survival (OS) and progression-free survival (PFS)^{18,19}. These results warranted approval of the doublet therapy as a new standard therapy for CRC^{BRAF-V600E} by the US Food and Drug Administration and European Medicines Agency²⁰. While the responses documented are unprecedented for patients with mCRC^{BRAF-V600E}, these still compare unfavorably with the higher response rates observed in *BRAF*-mutant metastatic melanomas treated with anti-BRAF therapy^{9,10} and display a high degree of heterogeneity, which underscores the need for a deeper understanding of factors modulating treatment response that can optimize the clinical management of patients^{1,21}.

Herein we sought to explore genetic biomarkers with a predictive value that can contribute to refining the stratification of patients with mCRC^{BRAF-V600E} treated with anti-BRAF/EGFR combinatorial therapy. We applied whole-exome sequencing (WES) and/or targeted gene sequencing on baseline tumor and/or plasma cell-free DNA (cfDNA) samples from a large cohort of patients with mCRC^{BRAF-V600E} treated with anti-BRAF/EGFR therapy, as well as from a control cohort of patients with mCRC^{BRAF-V600E} receiving standard chemotherapies and antiangiogenic agents (and not exposed

to anti-BRAF), and integrated these data with clinical correlates of response and survival. Our findings identified molecular subtypes based on microsatellite-stable (MSS)/MSI status and *RNF43* alterations and uncovered the predictive value of *RNF43* mutations as a biomarker of clinical outcome, including increased ORR, PFS and OS, to anti-BRAF/EGFR ± combinatorial therapies. Specifically, our data show that patients with MSS-mCRC^{BRAF-V600E} tumors harboring loss-of-function mutations in *RNF43* respond favorably to anti-BRAF/EGFR combinatorial therapy, whereas those with functional *RNF43* derived limited benefit from this regimen (Fig. 1).

Results

Description of patient cohorts treated with anti-BRAF/EGFR.

A total of 98 patients with mCRC^{BRAF-V600E} treated with anti-BRAF/EGFR ± combinatorial therapies in clinical trials or who received such therapies through a compassionate use program were included in the current study (Fig. 1 and Extended Data Fig. 1b). The discovery cohort was composed of 46 patients from the Vall d'Hebron University Hospital (Barcelona, Spain) prospectively included from 2013 to 2021, and the validation cohort comprised 52 patients from three academic hospitals from Italy (Fondazione IRCCS Istituto Nazionale dei Tumori, Milan, Italy; University Hospital of Pisa, Pisa, Italy; Istituto Oncologico Veneto IOV-IRCCS, Padova, Italy).

In the discovery cohort, 28 patients (61%) were female, with a median age at diagnosis of 61 years (range, 33–82 years), 31 patients (67%) had right-sided tumors, 34 patients (74%) had more than one

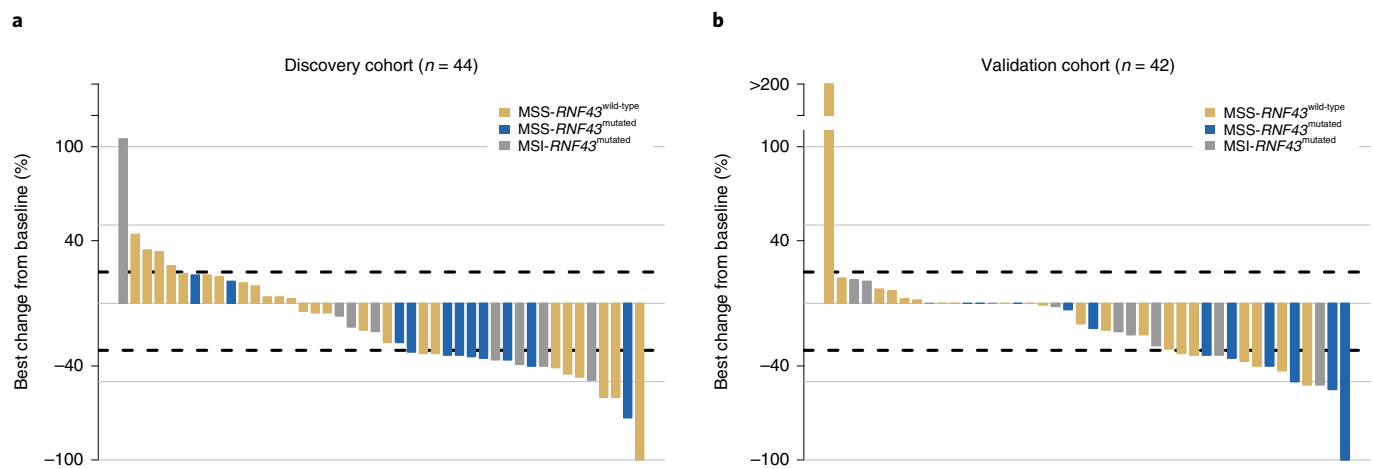


Fig. 2 | Clinical responses to BRAF/EGFR inhibition according to MSS/MSI and *RNF43* status. **a, b**, Waterfall plots representing best observed response in the mCRC^{BRAF-V600E} discovery cohort ($n = 44$) (**a**) and validation cohort ($n = 42$) (**b**), measured as percentage best change from baseline according to RECIST 1.1 criteria²² (Methods). Colors refer to molecular subtypes: MSS-*RNF43*^{wild-type} tumors (yellow), MSS-*RNF43*^{mutated} tumors (blue) and MSI-*RNF43*^{mutated} tumors (gray).

metastatic site, and 37 patients (80%) had MSS and 9 patients (20%) had MSI tumors. In total, 35 patients (76%) received anti-BRAF/EGFR-based combinations as second- or third-line therapy, 6 patients (13%) received this as first-line therapy and 5 patients (11%) received this beyond third-line therapy. The number of patients who received the doublet combination was 29 (63%), and 17 patients (37%) received the triplet combination. The ORR by Response Evaluation Criteria in Solid Tumors version 1.1 (RECIST 1.1; ref. ²²) was 44% (20/45 patients, one patient was not evaluable for response). The number of patients with MSI tumors who received immunotherapy after targeted therapy was 3 (7%). The *RNF43* mutation frequency was 43% (20/46) in the overall discovery cohort, 100% (9/9, all G659fs) in MSI tumors and 30% (11/37) in MSS tumors (Supplementary Table 1 and Fig. 2a).

In the validation cohort, 31 patients (60%) were female, with a median age at diagnosis of 62 years (range, 38–80 years), 40 patients (77%) had right-sided tumors, 33 patients (63%) had more than one metastatic site, and 39 patients (75%) had MSS and 13 patients (25%) had MSI tumors. Overall, 33 (63%) patients received anti-BRAF/EGFR-based combinations as second-line therapy, and 19 patients (37%) received this as third-line therapy. The number of patients who received the doublet combination was 29 (56%), and 23 patients (44%) received the triplet combination. The ORR by RECIST 1.1 (ref. ²²) was 27% (14/51 patients, one patient was not evaluable for response). Six patients (12%) with MSI tumors received immunotherapy after targeted therapy. The *RNF43* mutation frequency was 44% (23/52) in the overall validation cohort, 92% (12/13, G659fs) in MSI tumors and 28% (11/39) in MSS tumors (Supplementary Table 1 and Fig. 2b).

Biomarkers of response to anti-BRAF/EGFR in MSS-mCRC^{BRAF-V600E}. WES analysis detected mutations in several cancer-related genes previously reported to be implicated in mCRC^{BRAF-V600E} tumors, such as *APC*, *TP53*, *ARID1A*, *PIK3CA*, *FBXW7* and *RNF43*, among others (Supplementary Table 2). In general, the mutation frequencies of the discovery cohort were comparable to those observed in The Cancer Genome Atlas (TCGA) CRC tumors carrying the *BRAF*^{V600E} mutation from the PanCancer Atlas^{23,24} ($n = 46$; Supplementary Table 2). Unbiased maximum-likelihood analysis of WES mutational data from responders (partial response (PR) and complete response (CR)) versus nonresponders (stable disease (SD) and progressive disease

(PD)) using dNdScv²⁵ identified the *RNF43* gene as a top candidate gene associated with ORR (P values and q values < 0.001 ; Extended Data Fig. 2a,b). Other candidate genes were identified, but we focused on *RNF43* because of its high mutation frequency and implications in CRC biology. *RNF43* mutations were detected in both tumor-derived and plasma cfDNA-derived DNA samples (Extended Data Fig. 3a–c).

The mutation rate of *RNF43* in the discovery cohort (20/46, 43%) was consistent with the rate reported in the TCGA PanCancer Atlas for CRC^{BRAF-V600E} (refs. ^{23,24}, 21/46, 46%). To test the potential association between *RNF43* mutations and ORR, we analyzed data from the whole discovery series including WES and next-generation sequencing (NGS) panel data from 45 evaluable patients with mCRC^{BRAF-V600E}. ORR in the whole *RNF43*^{mutated} subgroup, including MSS and MSI tumors, was 63% (12/19), which was significantly superior to the ORR of 31% achieved in patients with *RNF43*^{wild-type} status (8/26; $P = 0.03$; Extended Data Fig. 4a). The accuracy of *RNF43* mutations alone for predicting response to treatment was 67% (sensitivity, 60%; specificity, 72%; positive predictive value (PPV), 63%; negative predictive value (NPV), 69%; Extended Data Fig. 4g). In line with findings in the BEACON trial, patients with MSS and MSI CRC^{BRAF-V600E} achieved similar ORRs (50% (4/8) versus 43% (16/37); $P = 1$; Extended Data Fig. 4b), and the predictive accuracy of MSS/MSI status alone was 44% (sensitivity, 80%; specificity, 16%; PPV, 43%; NPV, 50%; Extended Data Fig. 4g).

We next classified tumor samples according to three molecular subtypes: MSS-*RNF43*^{wild-type}, MSS-*RNF43*^{mutated} and MSI-*RNF43*^{mutated}. The ORR of the MSS-*RNF43*^{mutated} subtype was significantly higher than those of the MSS-*RNF43*^{wild-type} and MSI-*RNF43*^{mutated} subtypes (73% versus 31% and 50%, respectively; $P = 0.03$) (Fig. 2a and Extended Data Fig. 4c). In agreement, accuracy for prediction of response combining MSS/MSI + *RNF43* mutation status was 67% (sensitivity, 40%; specificity, 88%; PPV, 73%; NPV, 65%; Extended Data Fig. 4g).

Validation of MSS/MSI-*RNF43* status and clinical response. To explore the generalizability of the results obtained in the discovery set, we sought to validate the predictive value of *RNF43* mutations in an external independent cohort of patients treated with anti-BRAF/EGFR ± combinatorial therapies as second- or third-line therapy ($n = 52$). Overall, the ORR in the validation cohort was 27% (95% confidence interval (CI), 16.3–42%; 14/51 patients) with a

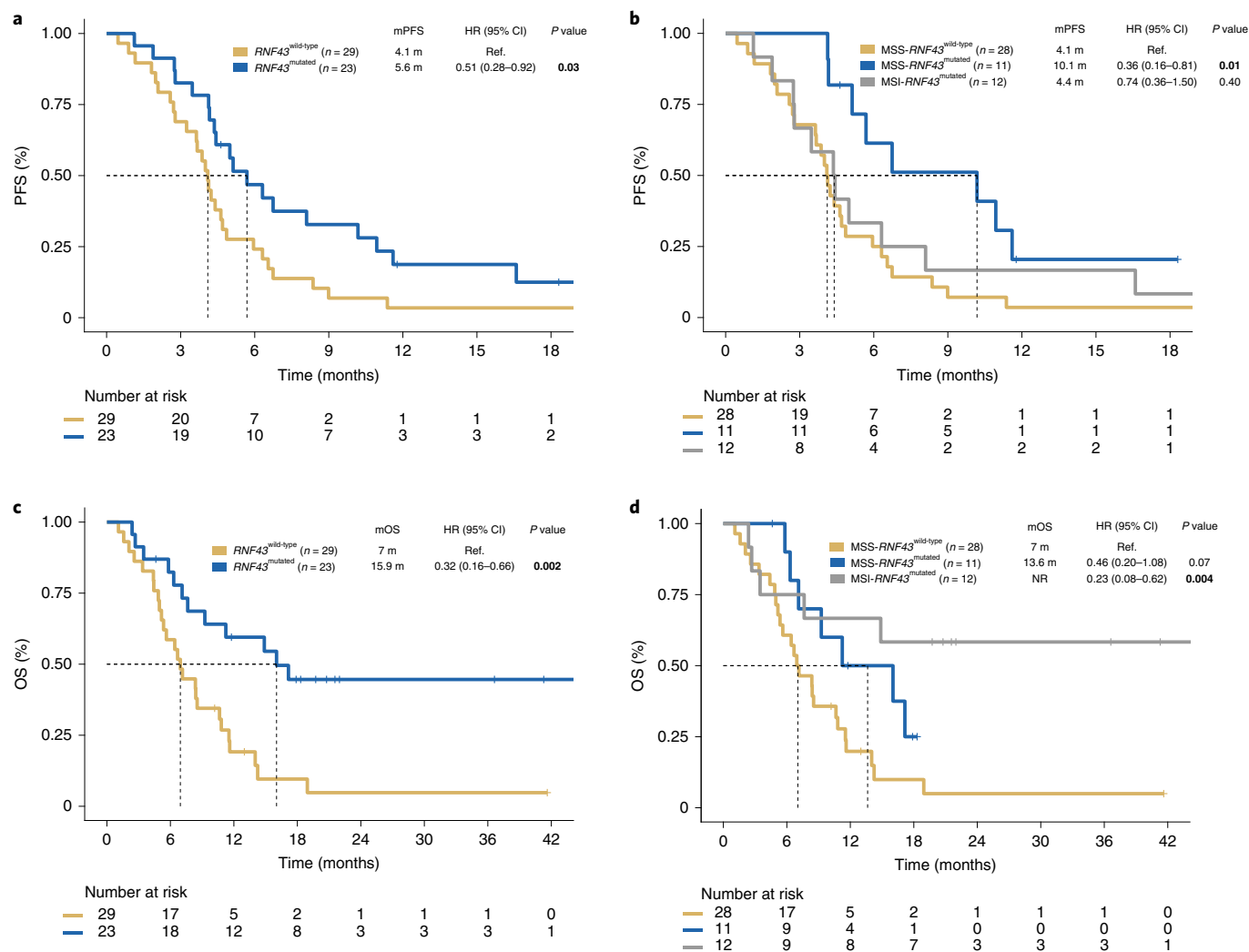


Fig. 3 | Survival analysis of patients undergoing BRAF/EGFR inhibition according to MSS/MSI and *RNF43* status. **a,b, Kaplan–Meier curves representing PFS of patients with *RNF43*^{wild-type} ($n = 29$) and *RNF43*^{mutated} ($n = 23$) tumors (**a**) and combined *RNF43* and MSS/MSI status (*MSS-RNF43*^{wild-type} ($n = 28$), *MSS-RNF43*^{mutated} ($n = 11$) and *MSI-RNF43*^{mutated} ($n = 12$)) (**b**). **c,d**, OS of patients with *RNF43*^{wild-type} ($n = 29$) and *RNF43*^{mutated} ($n = 23$) tumors (**c**) and combined *RNF43* and MSS/MSI status (*MSS-RNF43*^{wild-type} ($n = 28$), *MSS-RNF43*^{mutated} ($n = 11$) and *MSI-RNF43*^{mutated} ($n = 12$)) (**d**). Cox models were used to obtain HRs with 95% CIs, and the two-sided log-rank test was used for statistical comparisons without adjustment for multiplicity. Colors indicate molecular subtypes: *RNF43*^{wild-type} tumors with or without MSS (yellow), *RNF43*^{mutated} tumors with or without MSS (blue) and *MSI-RNF43*^{mutated} tumors (gray). Significant values are shown in bold. m, months; NR, not reported; Ref., reference.**

median PFS (mPFS) of 4.4 months (95% CI, 4.1–5.9 months) and a median OS (mOS) of 8.5 months (95% CI, 6.9–14.2 months) (Supplementary Table 1). Consistent with the results in the discovery cohort, patients in the *MSS-RNF43*^{mutated} subtype in the validation cohort also achieved a significantly higher ORR compared to those in the *MSS-RNF43*^{wild-type} and *MSI-RNF43*^{mutated} subtypes (54% versus 21% and 18%, respectively; $P = 0.02$; Fig. 2b and Extended Data Figs. 4d–f and 5a–d).

We next evaluated whether the observed increased ORR was a surrogate for improved outcomes measured by PFS and OS. The mPFS in the *MSS-RNF43*^{mutated} subtype was 10.1 months (hazard ratio (HR), 0.36; 95% CI, 0.16–0.81), 4.1 months in the *MSS-RNF43*^{wild-type} subtype and 4.4 months (HR, 0.74; 95% CI, 0.36–1.50) in the *MSI-RNF43*^{mutated} subtype (Fig. 3a,b and Extended Data Fig. 6a,b). The *MSS-RNF43*^{mutated} subtype also showed a trend toward better OS compared to the *MSS-RNF43*^{wild-type} subtype (mOS of 13.6 versus 7 months; $P = 0.07$; HR, 0.46; 95% CI, 0.20–1.08; Fig. 3c,d and Extended Data Fig. 6c,d). In multivariate analysis, the

MSS-RNF43^{mutated} subtype maintained an independent association with OS (HR, 0.26; 95% CI, 0.10–0.71; $P = 0.008$) after adjusting for imbalance in prognostic factors such as age and metastatic site (Fig. 4a,b). Despite having a short PFS in response to anti-BRAF/EGFR therapies, patients with *MSI-RNF43*^{mutated} status did not show a significantly lower mOS when compared to those with *MSS-RNF43*^{mutated} status, most likely because of the positive impact of the treatment with immune-checkpoint inhibitors administered in six patients (12%) with MSI after progression on anti-BRAF/EGFR therapy (HR, 0.38; 95% CI, 0.09–1.48; $P = 0.16$; Fig. 4b).

We also sought to explore whether, in addition to their power to predict response, the MSS/MSI-*RNF43* molecular subtypes could anticipate refractoriness to anti-BRAF/EGFR ± combinatorial therapies. Of the 16 patients with refractory mCRC^{BRAF-V600E} in the discovery and validation cohorts with PD as the best observed response, 13 (13/16, 81%) were *MSS-RNF43*^{wild-type}, 3 (3/16, 19%) were *MSI-RNF43*^{mutated} and none (0/16, 0%) were *MSS-RNF43*^{mutated}. Strikingly, none of the 22 patients with

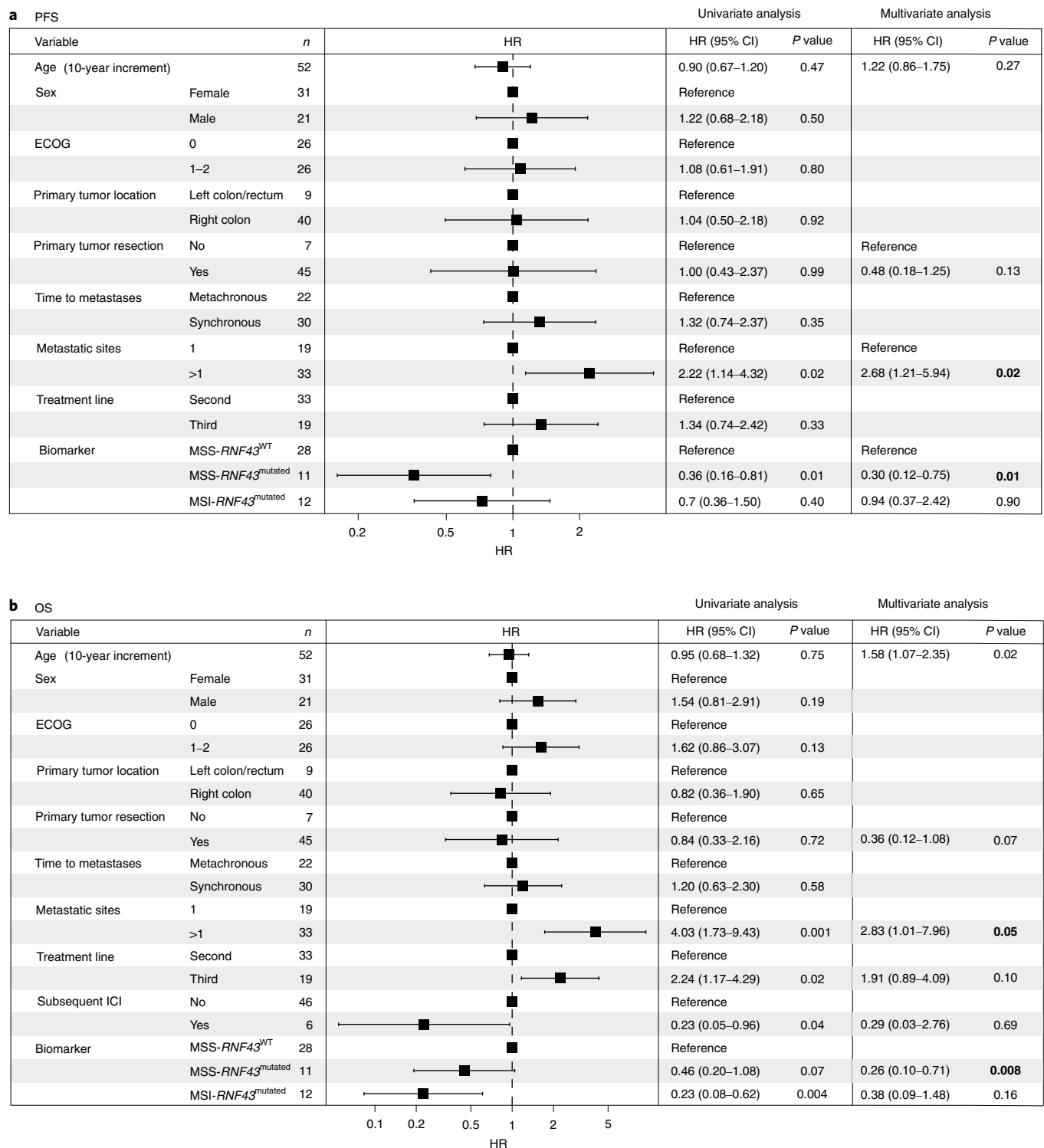


Fig. 4 | Univariate and multivariate Cox regression models. a,b. Analysis performed in the validation cohort ($n=52$) for PFS (**a**) and OS (**b**). Univariate HRs along with 95% CIs are represented for each prognostic factor. *P* values were estimated by means of the two-sided log-rank test in the univariate analysis and by means of the Cox model in the multivariate analysis (two-sided). Significant values are shown in bold. ECOG, Eastern Cooperative Oncology Group performance; ICI, immune checkpoint inhibitor.

MSS-*RNF43*^{mutated} status in the two cohorts had PD as the best response (Extended Data Fig. 5d).

Predictive value of *RNF43* mutations in MSS-mCRC^{BRAF-V600E}. To further confirm the value of *RNF43* mutations in predicting response

to treatment in patients with MSS-mCRC^{BRAF-V600E} tumors, we aggregated data from 68 sex- and age-matched patients treated in four different hospitals (Extended Data Fig. 7a–e). All patients received standard-of-care chemotherapies and antiangiogenic agents that did not involve anti-BRAF therapy. The median age at diagnosis

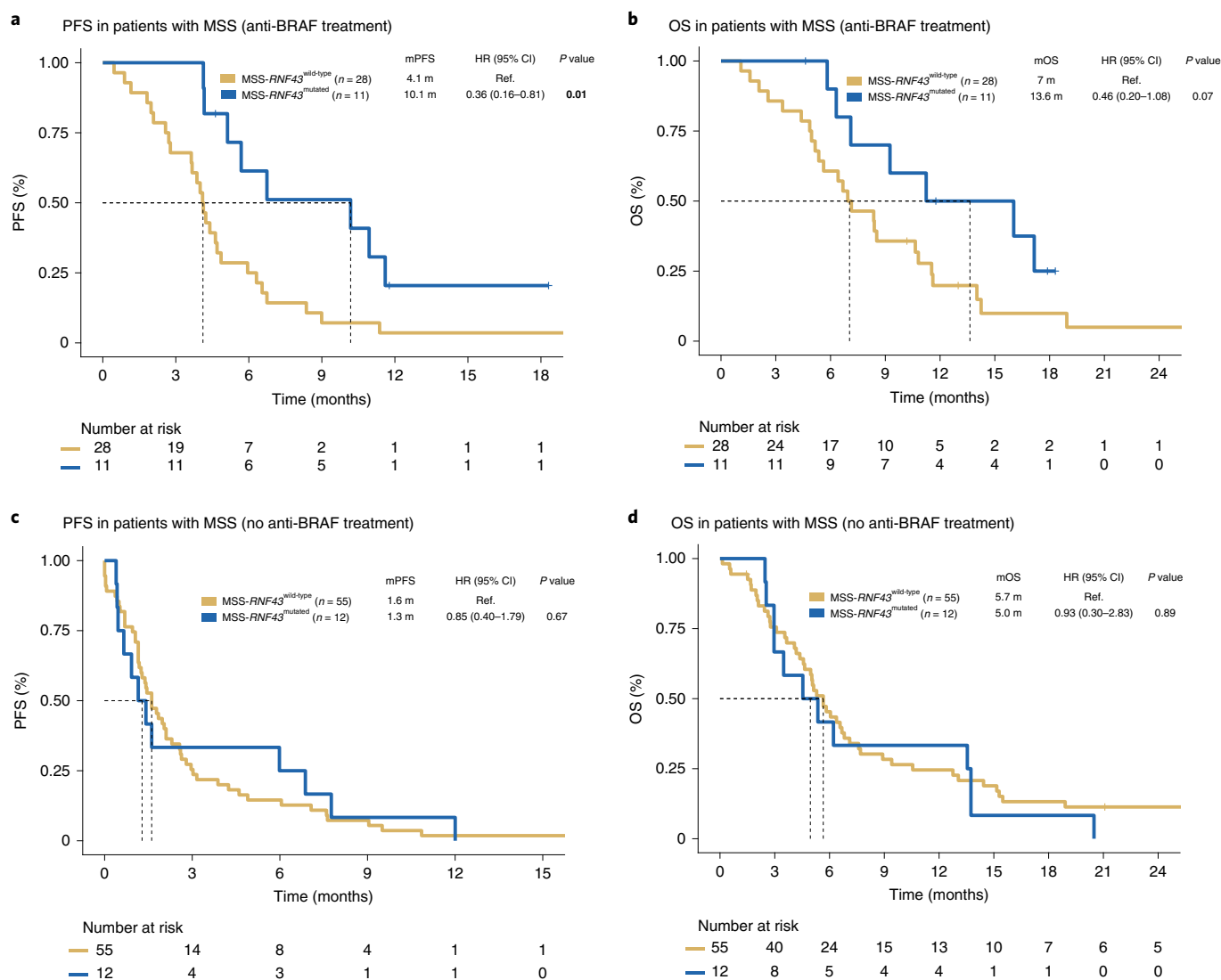


Fig. 5 | Predictive value of MSS/MSI-*RNF43* status. **a–d**, Kaplan–Meier curves representing PFS (**a**) and OS (**b**) for patients with mCRC^{BRAF-V600E} undergoing anti-BRAF/EGFR therapy in the validation cohort (anti-BRAF/EGFR as second or third line, $n = 39$) and PFS (**c**) and OS (**d**) in patients in the control cohort not exposed to BRAF inhibition ($n = 67$ second and third treatment lines; Extended Data Fig. 7). Cox models were used to obtain HRs with 95% CIs, and the two-sided log-rank test was used for statistical comparisons without adjustment for multiplicity. Colors refer to molecular subtypes: MSS-*RNF43*^{wild-type} (yellow) and MSS-*RNF43*^{mutated} (blue). Significant values are shown in bold.

was 60.5 years (range, 30–80 years); 68% of patients had right-sided tumors. With regard to MSS/MSI-*RNF43* status, 22% of patients were MSS-*RNF43*^{mutated} and 78% were MSS-*RNF43*^{wild-type}, similar to the discovery and validation MSS tumor cohorts (29% and 71%, respectively) (Extended Data Fig. 7a–c and Supplementary Table 1). Moreover, the MSS discovery/validation and control cohorts presented with similar *RNF43* mutation frequencies (29% (22/76) and 22% (15/68), respectively) (Extended Data Fig. 7b,c) as well as *RNF43* mutation localization patterns (Extended Data Fig. 7d,e). Among 68 patients treated in the second- and third-line setting, those in the MSS-*RNF43*^{mutated} subgroup achieved a mPFS of 1.3 months as compared to 1.6 months in the MSS-*RNF43*^{wild-type} population (HR, 0.85; 95% CI, 0.40–1.79; $P = 0.67$). Similarly, we found no differences in mOS after the start of second-line therapy (5 months in patients with MSS-*RNF43*^{mutated} tumors and 5.7 months in patients with MSS-*RNF43*^{wild-type} tumors; HR, 0.93; 95% CI, 0.30–2.83; $P = 0.89$) (Fig. 5a–d). To corroborate these findings, we also evaluated mPFS in the first-line setting for the entire control cohort and found no significant differences in the MSS-*RNF43*^{mutated}

versus MSS-*RNF43*^{wild-type} population (4.5 months versus 3.9 months, respectively; HR, 0.64; 95% CI, 0.36–1.15; $P = 0.13$) (Extended Data Fig. 8a–d). Altogether, these data suggest that *RNF43* mutations have no prognostic relevance in patients with MSS-mCRC^{BRAF-V600E} in our cohort and support their predictive value in response to anti-BRAF/EGFR combinatorial therapies in this clinical setting. Conversely, the predictive value of *RNF43* mutations seen in MSS tumors was not observed in MSI tumors.

Molecular profiles of *RNF43* mutations in mCRC^{BRAF-V600E}. To better understand the underlying molecular features of MSS-*RNF43*^{mutated} CRC^{BRAF-V600E} tumors, we next classified and characterized the observed *RNF43* somatic mutations occurring in patients from both the discovery and validation cohorts. *RNF43* mutations were identified in 21 of 22 (95%) MSI tumors and 22 of 76 (29%) MSS tumors. In addition to the different frequencies, the location and functional nature of the *RNF43* mutations were fundamentally distinct in MSI and MSS tumors (Fig. 6a). All MSI *RNF43*-mutated tumors carried a hotspot mutation

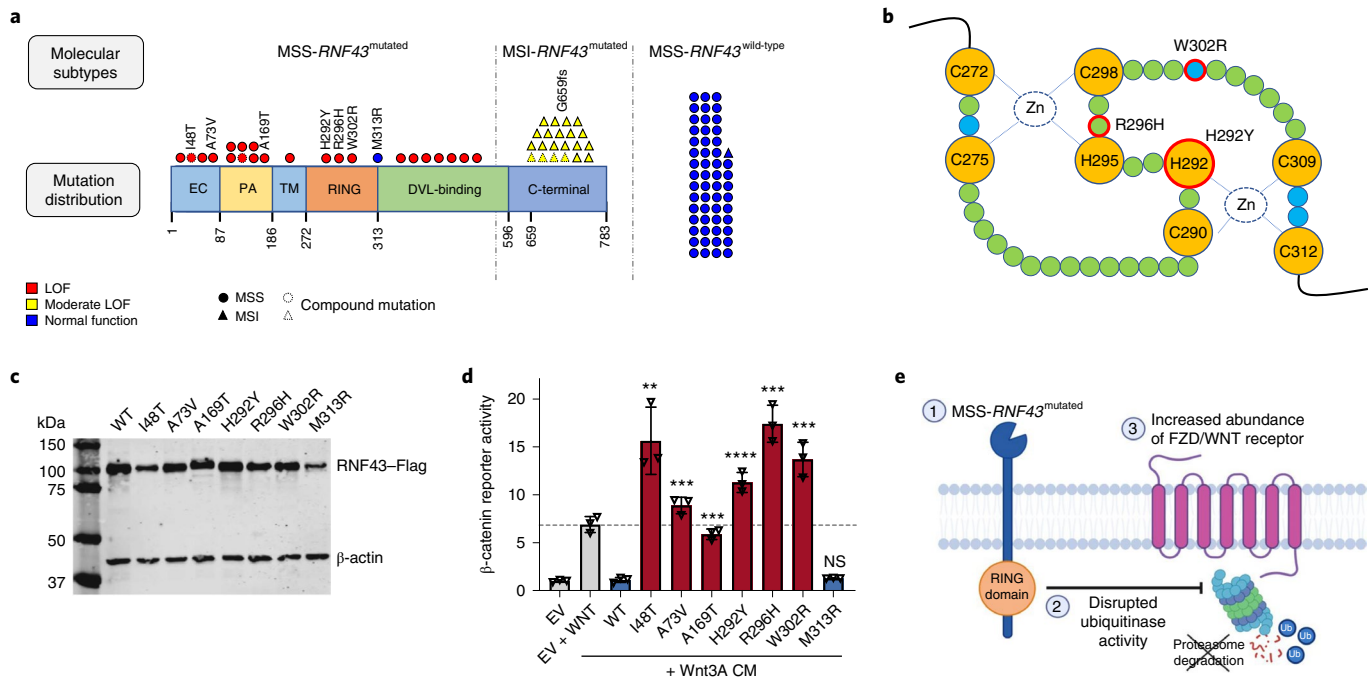


Fig. 6 | Functional analysis of *RNF43* mutations. **a**, Distinct localization and functional impact of *RNF43* mutations among patients with mCRC^{BRAF-V600E} treated with anti-BRAF/EGFR therapy according to MSS/MSI and *RNF43* molecular status ($n=98$). MSI CRCs ($n=21$) carried a mutation encoding G659fs, while MSS CRCs were divided into MSS-*RNF43*^{mutated} ($n=22$) and MSS-*RNF43*^{wild-type} ($n=54$) tumors. Numbers indicate the amino acid residue in the *RNF43* protein sequence. The MSS-*RNF43*^{mutated} subtype harbored mutations mainly in the *RNF43* N-terminal domain. Colors indicate the effect of the mutation on protein function: loss of function (LOF) (red), moderate loss of function (yellow) and normal function (blue); symbols reflect MSS/MSI status (circle and triangle, respectively) and the presence of a compound mutation (discontinuous border). **b**, Illustration of the ‘cross-brace’ topology of the RING domain containing a highly conserved sequence of cysteine-histidine residues that coordinates two atoms of zinc and four hydrophobic residues that are involved in binding to E2 (canonical sequence, CX₂CX_(9–39)CX_(1–3)HX_(2–3)CX₂CX_(4–48)CX₂C). Figure adapted from ref. ³⁶, Frontiers Media (CC BY 4.0 license). Mutations encoding H292Y, R296H and W302R in the RING domain of *RNF43* are circled in red, while the mutation encoding M313R is located right outside the RING protein domain and likely for this reason did not affect *RNF43*’s ubiquitinase function. The four conserved residues are shown in blue. **c**, Western blot quantification of Flag-tagged *RNF43* protein ectopically expressed in the HEK293T cell line; β -actin, loading control. This experiment was repeated twice obtaining the same protein expression levels. **d**, In vitro luciferase reporter assays representing levels of β -catenin activation (y-axis) upon ectopic expression of *RNF43* mutants (x-axis) in HEK293T cells, following stimulation with Wnt3A conditioned medium (CM). One representative experiment is shown. The assay was performed three times with basically identical results. The statistical significance of all mutants relative to wild-type protein was obtained using a two-sided Student’s *t*-test (** $P < 0.01$, *** $P < 0.001$, **** $P < 0.0001$; NS, not significant). Empty vector (EV) and EV + WNT (control conditions) are shown in gray, *RNF43* alterations that behaved as loss-of-function variants are shown in red and wild-type protein and the M313R variant are shown in blue. **e**, Graphical representation of the impact of *RNF43* mutations (1) in impairing the ubiquitinase activity of the protein (2), resulting in the accumulation of FZD/WNT receptors in the cell membrane (3). Ub, ubiquitin.

encoding p.G659fs*41 at the C-terminal, which is caused by a DNA slippage error at the seven-guanine repeat region, typical in MSI tumors lacking full DNA repair machinery, and classified as moderate loss of function with retained wild-type-like functional properties²⁶. Conversely, the mutations occurring in MSS tumors were not recurrent and spanned the N-terminal domain of the protein, including the extracellular (EC), protease-associated (PA), transmembrane (TM), RING finger (RING) and DVL2-binding (DVL) domains. We identified 7 missense mutations in these domains and 16 that led to protein truncations predicted to cause loss of function^{27,28} (Fig. 6a,b). To validate the biological impact of the *RNF43* missense mutations detected in the MSS-mCRC^{BRAF-V600E} tumors of our patients, we performed luciferase reporter assays^{27,28}. Compared to wild-type *RNF43*, six of seven (86%) of the *RNF43* mutations analyzed (encoding I48T, A73V, A169T, H292Y, R296H and W302R substitutions) behaved as loss-of-function variants (Fig. 6c,d). The corresponding inactivated *RNF43* mutants lost the capacity to ubiquitinate and degrade FZD/WNT receptors, resulting in an accumulation of these receptors on the cell membrane and in high WNT signal levels in the luciferase reporter assays (Fig. 6c–e). Because of

this effect, *RNF43* loss-of-function mutations are also referred to as ‘WNT-hyperactivating’ mutations^{26–28}.

Mutations detected in other genes of the WNT pathway, such as *APC* and *CTNNB1*, are shown in Supplementary Table 1 and did not correlate with ORR (Extended Data Fig. 9a,b). Moreover, no correlation was observed of β -catenin protein expression levels and localization with response to anti-BRAF/EGFR \pm combinatorial therapies, MSS/MSI status or *RNF43* mutation status in 33 mCRC^{BRAF-V600E} tumors from the discovery cohort (Extended Data Fig. 9c,d).

Discussion

mCRC^{BRAF-V600E} represents an entity of its own with particular phenotypic features and with crucial implications in terms of prognosis^{2,3}. Hence, there is a critical need for new clinical–biological insights that can lead to therapeutic improvements and the identification of new biomarkers of response. However, identification of biomarkers in this patient population, as well as development of new therapeutic strategies, has been challenging in this particular tumor type, given its underrepresentation in randomized clinical

trials due to its low frequency (up to 12% of mCRC) and the high tumor burden and poor clinical conditions that impair inclusion of these patients in clinical trials²⁹. Indeed, some of the current recommendations for standard-of-care treatments are based on subgroup analyses of phase 3 clinical trials^{3,30,31}. On the other hand, despite the meaningful clinical activity observed in clinical trials evaluating BRAF inhibitor-based combinations, not all patients respond the same, and some responses are relatively short. This disparity in terms of treatment benefit highlights the biological heterogeneity of mCRC^{BRAF-V600E} and justifies better molecular characterization to optimize treatment outcomes.

Through pursuing an unbiased genomic analysis of responders versus nonresponders, we detected a strong signal in the *RNF43* locus in association with clinical outcome in response to anti-BRAF/EGFR-based therapies that was confirmed in a validation cohort (Fig. 3a–d) but not observed in a sex- and age-matched control cohort of patients receiving standard chemotherapy ± antiangiogenic agents (Fig. 5a–d and Extended Data Fig. 8a–d). Our study uncovers a previously unknown value of *RNF43* mutations, occurring in 29% of MSS-mCRC^{BRAF-V600E} tumors, in predicting response and clinical outcome. In contrast to patients with MSI mCRC, the patient population with MSS-mCRC^{BRAF-V600E} currently lacks biomarkers to guide treatment decision-making. Although previous analyses had associated tumor-based transcription subtypes with response³², our study reports a potential genomic prediction biomarker to anti-BRAF/EGFR-based combinations in the patient population with mCRC^{BRAF-V600E}. Specifically, we found that within the MSS group, which represents 70% of patients with mCRC^{BRAF-V600E}, the occurrence of a *RNF43* mutation was associated with improved ORR and, importantly, longer PFS and OS with anti-BRAF/EGFR strategies (Figs. 2a,b, 3a–d and 5a–d and Extended Data Figs. 4a–g and 5a–f).

Overall, this finding has two main implications. First, incorporating *RNF43* mutation as a routine biomarker could contribute to defining the optimal treatment sequence in patients with MSS-mCRC^{BRAF-V600E} according to their predicted response profile. Second, it uncovers a cross-talk between MAPK and RNF43–WNT pathways in the antitumor activity of BRAF/EGFR-targeting therapy, which might be exploited as a future potential therapeutic target.

The mechanistic basis underlying the clinical success of concomitant BRAF/EGFR inhibition builds upon preclinical evidence of a rapid feedback compensation for EGFR mediated by the activation of CRAF or by the transactivation of CRAF–BRAF heterodimers^{13,14}. Our findings underscoring the potential role of RNF43 in modulating response to anti-BRAF/EGFR therapy point to an interplay between the MAPK and WNT signaling pathways in MSS-mCRC^{BRAF-V600E} tumors. Specifically, our *in vitro* experiments show that most *RNF43* mutations detected in MSS tumors of responding patients have a loss-of-function effect, which contrasts with *RNF43* mutations described in MSI tumors, where the protein retains its function²⁶. In our patient datasets, loss of RNF43 would impair degradation of WNT/FZD receptors, leading to activation of the WNT pathway. While the molecular intricacies through which the MAPK and WNT pathways cross-talk to modulate the antitumor activity of this treatment combination need to be studied in detail, our clinical findings are consistent with preclinical studies describing a role for WNT activation in antagonizing MAPK-driven proliferation to preserve an equilibrium with differentiation of intestinal stem cells³³. It is therefore plausible to speculate that a similar mechanism of RNF43 loss-dependent WNT activation may be restraining MAPK signaling in MSS mCRC tumors and synergizing with pharmacological blockade of the pathway. Of note, we found no correlation of response with the presence of *APC* or *CTNGB1* mutations or β -catenin protein expression or localization in mCRC^{BRAF-V600E} tumors (Extended Data Fig. 9a–d and Supplementary Table 1),

suggesting that noncanonical WNT pathways^{34,35}, rather than canonical (β -catenin-dependent) signaling, might be involved in modulation of anti-BRAF/EGFR activity.

Despite our study representing, to our knowledge, the largest genetic biomarker analysis to date on this patient population, the overall number of patients remains limited owing to the rarity of *BRAF*^{V600E} mutation in mCRC and the difficulties in accessing clinically annotated cohorts with comprehensive genomic profiling. Furthermore, while our genomic analyses uncover a robust association of *RNF43* mutations with clinical outcome, the inherent heterogeneity of our real-world patient cohorts receiving treatment in four different hospitals and undergoing molecular profiling with different multigene panels represents another limitation to be addressed in prospective, standardized biomarker studies. The lack of randomized data represents a constraint for analysis of the predictive versus prognostic role of *RNF43* mutations. In this regard, our efforts to identify control patients exposed to chemotherapies and antiangiogenic agents during the same time period and at the same hospitals that contributed data for the discovery and validation cohorts are the best mitigation available, also taking into account that similar NGS platforms were used for molecular stratification. Finally, despite our *in vitro* analysis supporting a loss-of-function effect of most *RNF43* mutations detected in MSS tumors from responding patients, the mechanistic basis for how altered WNT signaling modulates MAPK pathway activation in response to anti-BRAF/EGFR agents remains to be fully elucidated.

In summary, *RNF43* mutations represent a new biomarker that warrants further validation for its potential to help prioritize anti-EGFR/BRAF combinations in selected patients with mCRC^{BRAF-V600E} who are more likely to derive benefit and identify those patients for whom alternative treatment approaches are needed. Future research should explore incorporating this biomarker in routine testing along with *BRAF* and MSS/MSI status and evaluate their integration with other transcriptomic, microbiome or microenvironmental indicators for optimizing the clinical management of this heterogeneous and complex disease.

Online content

Any methods, additional references, Nature Research reporting summaries, source data, extended data, supplementary information, acknowledgements, peer review information; details of author contributions and competing interests; and statements of data and code availability are available at <https://doi.org/10.1038/s41591-022-01976-z>.

Received: 8 March 2022; Accepted: 26 July 2022;

Published online: 12 September 2022

References

- Di Nicolantonio, F. et al. Precision oncology in metastatic colorectal cancer—from biology to medicine. *Nat. Rev. Clin. Oncol.* **18**, 506–525 (2021).
- Morris, V. et al. Progression-free survival remains poor over sequential lines of systemic therapy in patients with *BRAF*-mutated colorectal cancer. *Clin. Colorectal Cancer* **13**, 164–171 (2014).
- Cremolini, C. et al. FOLFIRI plus bevacizumab versus FOLFIRI plus bevacizumab as first-line treatment of patients with metastatic colorectal cancer: updated overall survival and molecular subgroup analyses of the open-label, phase 3 TRIBE study. *Lancet Oncol.* **16**, 1306–1315 (2015).
- Yaeger, R. et al. Clinical sequencing defines the genomic landscape of metastatic colorectal cancer. *Cancer Cell* **33**, 125–136 (2018).
- Hoadley, K. A. et al. Cell-of-origin patterns dominate the molecular classification of 10,000 tumors from 33 types of cancer. *Cell* **173**, 291–304 (2018).
- Koo, B. K. et al. Tumour suppressor RNF43 is a stem-cell E3 ligase that induces endocytosis of Wnt receptors. *Nature* **488**, 665–669 (2012).
- Nusse, R. & Clevers, H. Wnt/ β -catenin signaling, disease, and emerging therapeutic modalities. *Cell* **169**, 985–999 (2017).
- Hyman, D. M. et al. Vemurafenib in multiple nonmelanoma cancers with *BRAF*^{V600} mutations. *N. Engl. J. Med.* **373**, 726–736 (2015).

9. Flaherty, K. T. et al. Inhibition of mutated, activated BRAF in metastatic melanoma. *N. Engl. J. Med.* **363**, 809–819 (2010).
10. Sosman, J. A. et al. Survival in *BRAF*^{V600}-mutant advanced melanoma treated with vemurafenib. *N. Engl. J. Med.* **366**, 707–714 (2012).
11. Kopetz, S. et al. PLX4032 in metastatic colorectal cancer patients with mutant BRAF tumors. *J. Clin. Oncol.* **28**, 3534 (2010).
12. Kopetz, S. et al. Phase II pilot study of vemurafenib in patients with metastatic BRAF-mutated colorectal cancer. *J. Clin. Oncol.* **33**, 4032–4038 (2015).
13. Prahallad, A. et al. Unresponsiveness of colon cancer to *BRAF*^{V600E} inhibition through feedback activation of EGFR. *Nature* **483**, 100–103 (2012).
14. Corcoran, R. B. et al. EGFR-mediated re-activation of MAPK signaling contributes to insensitivity of *BRAF* mutant colorectal cancers to RAF inhibition with vemurafenib. *Cancer Discov.* **2**, 227–235 (2012).
15. van Geel, R. et al. A phase Ib dose-escalation study of encorafenib and cetuximab with or without alpelisib in metastatic *BRAF*-mutant colorectal cancer. *Cancer Discov.* **7**, 610–619 (2017).
16. Kopetz, S. et al. Randomized trial of irinotecan and cetuximab with or without vemurafenib in *BRAF*-mutant metastatic colorectal cancer (SWOG S1406). *J. Clin. Oncol.* **39**, 285–294 (2021).
17. Ahronian, L. G. et al. Clinical acquired resistance to RAF inhibitor combinations in *BRAF*-mutant colorectal cancer through MAPK pathway alterations. *Cancer Discov.* **5**, 358–367 (2015).
18. Kopetz, S. et al. Encorafenib, binimetinib, and cetuximab in *BRAF*^{V600E}-mutated colorectal cancer. *N. Engl. J. Med.* **381**, 1632–1643 (2019).
19. Van Cutsem, E. et al. Binimetinib, encorafenib, and cetuximab triplet therapy for patients with *BRAF*^{V600E}-mutant metastatic colorectal cancer: safety lead-in results from the phase III BEACON colorectal cancer study. *J. Clin. Oncol.* **37**, 1460–1469 (2019).
20. Tabernero, J. et al. Encorafenib plus cetuximab as a new standard of care for previously treated *BRAF*^{V600E}-mutant metastatic colorectal cancer: updated survival results and subgroup analyses from the BEACON study. *J. Clin. Oncol.* **39**, 273–284 (2021).
21. Kopetz, S. et al. Molecular correlates of clinical benefit in previously treated patients (pts) with *BRAF*^{V600E}-mutant metastatic colorectal cancer (mCRC) from the BEACON study. *J. Clin. Oncol.* **39**, 3513 (2021).
22. Schwartz, L. H. et al. RECIST 1.1—standardisation and disease-specific adaptations: perspectives from the RECIST Working Group. *Eur. J. Cancer* **62**, 138–145 (2016).
23. Cerami, E. et al. The cBio cancer genomics portal: an open platform for exploring multidimensional cancer genomics data. *Cancer Discov.* **2**, 401–404 (2012).
24. Gao, J. et al. Integrative analysis of complex cancer genomics and clinical profiles using the cBioPortal. *Sci. Signal.* **6**, pl1 (2013).
25. Martincorena, I. et al. Universal patterns of selection in cancer and somatic tissues. *Cell* **171**, 1029–1041 (2017).
26. Tu, J. et al. The most common RNF43 mutant G659Vfs*41 is fully functional in inhibiting Wnt signaling and unlikely to play a role in tumorigenesis. *Sci. Rep.* **9**, 18557 (2019).
27. Yu, J. et al. The functional landscape of patient-derived *RNF43* mutations predicts sensitivity to Wnt inhibition. *Cancer Res.* **80**, 5619–5632 (2020).
28. Li, S. et al. Commonly observed *RNF43* mutations retain functionality in attenuating Wnt/ β -catenin signaling and unlikely confer Wnt-dependency onto colorectal cancers. *Oncogene* **39**, 3458–3472 (2020).
29. Van Cutsem, E., Cervantes, A., Nordlinger, B. & Arnold, D. Metastatic colorectal cancer: ESMO Clinical Practice Guidelines for diagnosis, treatment and follow-up. *Ann. Oncol.* **25**, iii1–iii9 (2014).
30. Van Cutsem, E. et al. Addition of aflibercept to fluorouracil, leucovorin, and irinotecan improves survival in a phase III randomized trial in patients with metastatic colorectal cancer previously treated with an oxaliplatin-based regimen. *J. Clin. Oncol.* **30**, 3499–3506 (2012).
31. Tabernero, J. et al. Ramucirumab versus placebo in combination with second-line FOLFIRI in patients with metastatic colorectal carcinoma that progressed during or after first-line therapy with bevacizumab, oxaliplatin, and a fluoropyrimidine (RAISE): a randomised, double-blind, multicentre, phase 3 study. *Lancet Oncol.* **16**, 499–508 (2015).
32. Middleton, G. et al. *BRAF*-mutant transcriptional subtypes predict outcome of combined BRAF, MEK, and EGFR blockade with dabrafenib, trametinib, and panitumumab in patients with colorectal cancer. *Clin. Cancer Res.* **26**, 2466–2476 (2020).
33. Kabiri, Z. et al. Wnt signaling suppresses MAPK-driven proliferation of intestinal stem cells. *J. Clin. Invest.* **128**, 3806–3812 (2018).
34. Tsukiyama, T. et al. A phospho-switch controls RNF43-mediated degradation of Wnt receptors to suppress tumorigenesis. *Nat. Commun.* **11**, 4586 (2020).
35. Radaszkiewicz, T. et al. RNF43 inhibits WNT5A-driven signaling and suppresses melanoma invasion and resistance to the targeted therapy. *eLife* **10**, e65759 (2021).
36. Garcia-Barcena, C., Osinalde, N., Ramirez, J. & Mayor, U. How to inactivate human ubiquitin E3 ligases by mutation. *Front. Cell Dev. Biol.* **8**, 39 (2020).

Publisher's note Springer Nature remains neutral with regard to jurisdictional claims in published maps and institutional affiliations.



Open Access This article is licensed under a Creative Commons Attribution 4.0 International License, which permits use, sharing, adaptation, distribution and reproduction in any medium or format, as long as you give appropriate credit to the original author(s) and the source, provide a link to the Creative Commons license, and indicate if changes were made. The images or other third party material in this article are included in the article's Creative Commons license, unless indicated otherwise in a credit line to the material. If material is not included in the article's Creative Commons license and your intended use is not permitted by statutory regulation or exceeds the permitted use, you will need to obtain permission directly from the copyright holder. To view a copy of this license, visit <http://creativecommons.org/licenses/by/4.0/>.

© The Author(s) 2022

Methods

Predictive and prognostic value analysis. To assess the predictive value of *RNF43* status, we aggregated the clinical and genetic data of 68 patients from four different cohorts (hospitals participating in the present work) treated with standard-of-care regimens only (no exposure to anti-BRAF therapies) whose tumors harbored *BRAF*^{V600E} mutation and with information on the status of MSI and *RNF43* mutations. These patients received in total 135 chemotherapy regimens with or without antiangiogenic drugs during the first, second or third line of therapy. To control for potential confounding factors, we excluded (1) treatments in the first line and (2) patients whose tumors were MSI and who received anti-PD1/PD-L1 therapies during the disease course. A total of 67 treatment lines (second and third line) in patients with MSS were analyzed. To compare the prognosis of patients with *MSS-RNF43*^{mutated} and *MSS-RNF43*^{wild-type} tumors, PFS and OS endpoints were estimated using the Kaplan–Meier method. Mixed-effects Cox models considering patient ID as a random effect, to adjust for the intra-patient variability in patients with more than one line of therapy, were used to obtain HRs with 95% CIs (Supplementary Table 1).

Ethics committee approval. The study was approved by each investigational site's institutional review board/ethics committee: Vall d'Hebron Institute of Oncology (VHIO), Barcelona, Spain; Veneto Institute of Oncology IRCCS, Padova, Italy; Azienda Ospedaliero-Universitaria Pisana, University of Pisa, Pisa, Italy; and Fondazione IRCCS Istituto Nazionale dei Tumori, Milan, Italy. The research was conducted in accordance with the Declaration of Helsinki and local data protection laws. All patients were provided with written informed consent before enrollment. All data provided are anonymized in line with applicable laws and regulations.

Radiological response evaluation. All cases were reviewed by board-certified radiologists with experience in oncology imaging and clinical trials. Radiological response for each patient was classified following the principles of RECIST 1.1 (ref. 22): CR (disappearance of the lesion or reduction in the short axis to <10 mm in the case of a pathological lymph node), PR (a decrease by at least 30% in the long axis for visceral or soft tissue disease and the short axis for pathological lymph nodes), PD (an increase of at least 20% in the long axis in the case of visceral or soft tissue disease and the short axis in the case of pathological lymph nodes) or SD (when the lesion did not fulfill the criteria for PR or PD). As is commonly the case in clinical practice for aggressive tumors, some patients included in the study had no image available due to evident progression as per rapid clinical deterioration, increase in the levels of tumor markers in plasma (CEA) and progression of nontarget disease. These patients were considered to have clinical PD.

DNA extraction. DNA extraction from tumor samples was performed with the automated system Maxwell 16 FFPE plus LEV DNA purification kit (Promega), and quality and concentration were measured with a NanoDrop 1000 spectrophotometer (Thermo Fisher Scientific). cfDNA was extracted from 1 ml of plasma using the QIAamp Circulating Nucleic Acid Kit (Qiagen), based on the manufacturer's recommendations, and quantified using the highly sensitive kit for the Qubit, dsDNA HS (High Sensitivity) Assay Kit (Thermo Fisher Scientific).

WES. WES was performed in 55 baseline biological samples available at VHIO's sample biobank (19 germline DNA, 22 tumor DNA, 5 patient-derived xenograft DNA and 9 plasma cfDNA) from 28 patients from the discovery cohort. Genomic libraries were prepared using 10–15 ng of cfDNA and the ThruPLEX DNA or Plasma-seq Kit (Rubicon Genomics; now commercialized as the SMARTer ThruPLEX plasma-seq kit by Takara Bio)^{37,38}. Quality control of libraries was carried out in TapeStation (Agilent), and amplified profiles of ~300 base pairs were considered for downstream analysis. Capture of the genomic coding regions for WES was performed using the SureSelect Human All Exon V5 or V6 kit (Agilent), with a target sequencing output of 12 Gb (100×) for genomic DNA and 36 Gb (300×) for tumor and cfDNA. Sequencing was carried out on a HiSeq or NovaSeq Illumina sequencing platform.

NGS cancer gene panel. Tumor samples from the discovery cohort that did not have WES data ($n = 18$) and from the validation ($n = 52$) and control ($n = 68$) cohorts were genetically analyzed using a VHIO in-house NGS test of 430 cancer genes or a Foundation Medicine or Caris Life Sciences commercial NGS platform³⁹.

Bioinformatics. Data processing and analysis (WES). The WES samples (FASTQ files) were processed using sarak (v2.7.1)⁴⁰. Briefly, the following steps were performed: quality filtering and adaptor trimming with TrimGalore; alignment to the reference genome with BWA; marking of duplicates with GATK4 MarkDuplicates; recalibration of scores with GATK4 BaseRecalibrator and ApplyBSQR; and computing of pileups with SAMtools. Variant calling was performed using four different tools: Mutect2, Strelka2, MSLSensor and Control-FREEC (tumor-only and pair mode). Filtering of the variants generated by Mutect2 was conducted using GATK4 GetPileupSummaries, CalculateContamination and FilterMutectCalls. Annotation of the variants was performed using snpEff. MultipleQC and statistics were generated using FastQC, Qualimap, SAMtools, VCFtools and MultiQC. We used a public Panel of Normals

(PON) obtained from the public repository of GATK at [gs://gatk-best-practices/somatic-hg38/1000g_pon.hg38.vcf.gz](https://gatk-best-practices/somatic-hg38/1000g_pon.hg38.vcf.gz) and a BED file containing all the genomic intervals of the kits used to generate the WES samples. Mutect2 variants corresponding to the tumor-only samples were refiltered with GATK4 FilterMutectCalls using a value of 10 for the parameter '-max-events-in-region'. These variants were subsequently reannotated with snpEff with the same genome reference, version and settings that were used in the processing pipeline. The generated mutational data were subsequently summarized, postprocessed, filtered and validated for downstream analysis.

Mutational enrichment analysis. Two different analyses were performed on the discovery cohort to determine which genes were enriched for somatic mutations in the responder and nonresponder groups. In the first analysis, we summarized the number of mutations, accumulated mutated allele frequency and number of samples/patients per gene. In the second analysis, we computed somatic enrichment *P* values and *q* values for each group using dNdScv²⁵ (GRCh38). This tool models the background mutation rate of each gene by combining local information (synonymous mutations in the gene) and global information (nonsynonymous mutations in the gene and other covariates) and controlling for the sequence composition of the gene and mutational signatures²⁵.

Functional classification of *RNF43* mutations. *Functional classification derived from previous in vitro and in vivo studies.* To initially assess the potential biological consequences of the identified *RNF43* mutations, we applied a recently developed functional classification derived from in vitro and in vivo studies^{26–28}. Accordingly, *RNF43* mutations can be classified as (1) wild-type like, (2) activators of the WNT- β -catenin pathway or (3) hyperactivators of the WNT- β -catenin pathway^{26–28}. Mechanistically, wild-type-like mutants maintain their capability to repress the WNT- β -catenin pathway and activators lose their ubiquitinase function, leading to an increased abundance of FZD/WNT receptors in the cellular membrane and activation of the WNT- β -catenin pathway, while hyperactivators exert a dominant-negative effect on the wild-type protein, completely blocking ubiquitination of FZD/WNT receptors and thereby leading to extremely high levels of WNT- β -catenin pathway activation^{26–28}.

*Luciferase reporter assays with *RNF43* mutation expression vectors.* To further demonstrate the biological impact of the identified *RNF43* missense mutations, we performed luciferase reporter assays with ectopic expression of the *RNF43* mutants. Flag-tagged *RNF43* mutation expression plasmids were generated using the New England Biolabs Q5 Mutagenesis Kit^{27,28}. All plasmids were full-length sequence verified.

HEK293T cells were used for the assays, cultured in DMEM (Gibco) supplemented with 10% (vol/vol) FBS (Gibco). Cells were cultured in a humidified incubator maintained at 37 °C with 5% CO₂. Cells tested negative for mycoplasma based on the real-time PCR method at Eurofins GATC-Biotech (Konstanz, Germany). Identity of the HEK293T cells was confirmed by the Erasmus Molecular Diagnostics Department, using PowerPlex-16 STR genotyping (Promega). For the β -catenin reporter assays, HEK293T cells were seeded in 24-well plates and transfected with 100 ng WRE Wnt/ β -catenin reporter, 100 ng *RNF43* expression plasmid (wild-type *RNF43*, mutant *RNF43* or empty vector) and 10 ng CMV-Renilla expression plasmid, using Lipofectamine 2000 (Thermo Fisher Scientific) as transfection reagent. L-Wnt3A or L-control conditioned medium (diluted 30-fold in normal growth medium) was added after 16 h. Cells were lysed in passive lysis buffer (Promega) 48 h after transfection. Next, the firefly and *Renilla* luciferase activity was measured with the Dual-Luciferase Reporter Assay System (Promega) using a LumiStar Optima luminescence counter (BMG LabTech). β -catenin reporter activity was measured in triplicate. All β -catenin reporter values were normalized to the value obtained for cells with empty vector exposed to L-control conditioned medium, which was arbitrarily set to 1. One representative experiment is shown. The assay was performed three times with basically identical results. Proper expression of Flag-tagged *RNF43* was analyzed using fluorescent western blotting as described below.

Immunoblotting analysis. Immunoblotting was carried out using standard methods. HEK293T cells transfected with *RNF43* were lysed in 2× Laemmli sample buffer with 0.1 M dithiothreitol and heated for 10 min at 95 °C. Proteins were separated by 10% SDS-PAGE and then transferred to an Immobilon-P PVDF membrane (MilliporeSigma). The membrane was blocked for 1 h with Odyssey Blocking Buffer (LI-COR Biosciences) at room temperature and incubated overnight with primary antibodies at 4 °C. After washing three times with 0.05% Tween-20 in TBS (TBST) buffer for 10 min, the membrane was incubated for 1 h with IRDye 680 Goat Anti-Mouse (1:1,000; LI 926-68070, LI-COR Biosciences) and then washed three times with TBST for 10 min. The membrane was scanned on the Odyssey Infrared Imaging System (LI-COR Biosciences). Primary antibodies used were mouse anti-FLAG (1:1,000; F1804, Sigma-Aldrich) and mouse anti- β -actin (1:1,000; sc-47778, Santa Cruz).

*Immunostaining of β -catenin in *CRC*^{BRAF-V600E} tumors.* Immunohistochemical analysis was performed using a primary antibody against human β -catenin

(prediluted, Beta-Catenin Mouse Monoclonal Antibody, clone 14, 760-4242, Cell Marque) in Benchmark ULTRA (Ventana Medical Systems). Labeling was performed using ULTRA Cell Conditioning 1 (ULTRACC1) (950-224, Roche) antigen retrieval buffer for 64 min at 95 °C, followed by incubation with primary antibody for 32 min at 36 °C and detection with the Ventana UltraView Universal DAB Detection Kit (760-500, Roche). Immunohistochemistry was scored semiquantitatively by one pathologist (R.E.) using an H-score (for the cytoplasm, membrane and nucleus separately). H-score was obtained by multiplying the proportion of cells showing cytoplasmic, membrane or nuclear staining and the intensity of staining (0, no staining; 1, weak; 2, moderate; 3, strong).

Statistical analysis. A descriptive analysis of all included variables in the study was performed. Continuous variables were expressed as the median and interquartile range, and categorical variables were expressed as absolute values and percentages. ORR was estimated in all subgroups based on RECIST version 1.1 criteria along with 95% CIs, and Fisher's exact test was used to assess statistical significance. Accuracy, sensitivity, specificity, and PPV and NPV were calculated to quantify the diagnostic performance of each potential biomarker.

PFS was defined as the time from anti-BRAF/EGFR therapy initiation to disease progression or death, whichever occurred first. OS was defined as the time from anti-BRAF/EGFR therapy initiation to death from any cause. PFS and OS were estimated using the Kaplan–Meier method and compared by the log-rank test. Cox proportional-hazard models were used to obtain HRs with 95% CIs. Formal statistical testing was only used in the validation cohort. No data imputation was performed. All tests were two sided with a value of $P < 0.05$ considered statistically significant without adjustment for multiple comparisons. All statistical analyses were performed using R statistical software.

Reporting summary. Further information on research design is available in the Nature Research Reporting Summary linked to this article.

Data availability

Reference genome GRCh38 was used for alignment. The FASTQ files corresponding to the WES data from clinical samples analyzed in the paper have been deposited in the European Genome-phenome Archive (EGA, <https://ega-archive.org>) under study ID [EGAS00001006247](https://ega-archive.org/study/EGAS00001006247) and dataset ID [EGAD000001008755](https://ega-archive.org/dataset/EGAD000001008755) with appropriate measures for controlled access (DUO: 0000020, DUO: 0000021). Further information about EGA can be found on <https://ega-archive.org>. “The European Genome-phenome Archive in 2021” (<https://academic.oup.com/nar/advance-article/doi/10.1093/nar/gkab1059/6430505>). Clinical and genetic data for the patients are available in Supplementary Table 1. Source data are provided with this paper.

Code availability

The code for the pipeline that was used to process all samples can be found at <https://github.com/nf-core/sarek>. Sarek is a Nextflow-based pipeline that integrates all the processing, mapping, variant calling and quality control steps²⁵. The code used for postprocessing, filtering, validation and analysis of the mutational data is available at <https://github.com/jfnavarro/scitron>.

References

- Toledo, R. A. et al. Exome sequencing of plasma DNA portrays the mutation landscape of colorectal cancer and discovers mutated VEGFR2 receptors as modulators of antiangiogenic therapies. *Clin. Cancer Res.* **24**, 3550–3559 (2018).
- Hastings, R. K. et al. Longitudinal whole-exome sequencing of cell-free DNA for tracking the co-evolutionary tumor and immune evasion dynamics: longitudinal data from a single patient. *Ann. Oncol.* **32**, 681–684 (2021).
- Randon, G. et al. Tumour mutational burden predicts resistance to EGFR/BRAF blockade in BRAF-mutated microsatellite stable metastatic colorectal cancer. *Eur. J. Cancer* **161**, 90–98 (2022).
- Garcia, M. et al. Sarek: a portable workflow for whole-genome sequencing analysis of germline and somatic variants. *F1000Res* **9**, 63 (2020).

Acknowledgements

VHIO would like to acknowledge the Cellex Foundation for providing research facilities and equipment, the FERO Foundation for their funding support, the Consorcio Centro de Investigación Biomédica en Red de Cáncer (CIBERONC, CB16/12/00259) from the Institute of Health Carlos III (ISCIII), Ministry of Science and Innovation, and the Department of Health (Generalitat de Catalunya, SLT008/18/00198 and SLT008/18/00205) for their support on this research. Authors acknowledge financial support from the State Agency for Research (Agencia Estatal de Investigación) (CEX2020-001024-S / AEI / 10.13039 / 501100011033). This research is funded by the SCITRON program; Novartis funded the genomics characterization by WES of samples from 28 patients from the discovery cohort and had no influence on data analysis/interpretation or writing of the paper (3003145512 to R.A.T.). S.Li. is financially supported by a Chinese Scholarship Council PhD fellowship (201909370083 to S. Li).

R.P.-L. is supported by a CRIS Foundation Talent Award (TALENT19-05), the FERO Foundation, the Instituto de Salud Carlos III-Investigación en Salud (PI18/01395 and PI21/01019 to R.P.-L.) and the Prostate Cancer Foundation (Young Investigator Award). This work was supported by the Miguel Servet-I Research Award from ISCIII of the Ministry of Economy (CP17/00199 to R.A.T.), the Olga Torres Foundation Award to emerging researchers (2601 to R.A.T.), the ISCIII-FEDER (PI17/00947 and PI20/00968 to E.E.), and the Fundación AECC (CLSEN19001ELEZ to E.E.) and Ministry of Science and Innovation (Europa Redes y Gestores, ECT2020-000827 to E.E.).

Author contributions

E.E., J.T. and R.A.T. conceived and designed the study. E.E., J.R., A.B.M.-C., C.A., A.G., P.N., R.I., A.M., M.M.G., G.R., C.C., S. Lonardi, F.P. and R.A.T. were involved in sample collection and data acquisition. E.E., J.R., J.F., A.B.M.-C., C.A., S. Li, R.F., A.V., R.S., C.C., S. Lonardi, F.P., R.D., J.T. and R.A.T. performed experiments, analysis and data interpretation. J.G.-R., A.P., D.P.K. and D.G. were involved in the project and study management. G.V., R.C. and R.D. performed the data and statistical analyses. K.B. and R.P.-L. performed the imaging and radiological analyses. A.B.M.-C. and A.V. performed genomic analyses. J.F. performed the bioinformatics analyses of the WES data and other computational analyses. G.K. performed computational analysis. C.A. and R.A.T. created Figs. 1 and 6e and Extended Data Figs. 1a, 2b and 3a with BioRender.com. R.A.T. wrote the manuscript, and E.E., J.R., R.S., A.B.M.-C., C.A., C.C., S. Lonardi, F.P., R.D. and J.T. participated in the review and editing. All authors approved the manuscript.

Competing interests

C.C. reports receiving honoraria and speaker's bureau compensation from Servier, Bayer, Merck, Amgen, Pierre Fabre, MSD, Roche and Nordic Pharma and research grants from Merck, Servier and Amgen. D.G. was an employee of Novartis and was a shareholder while this work was being conducted. D.P.K. is an employee of Novartis. E.E. reports receiving honoraria for an advisory role, travel grants and research grants (past 5 years) from Hoffmann-La Roche, Bristol-Myers Squibb, Servier, Amgen, Merck Serono, Array Biopharma, Sanofi and Bayer. Her institution received honoraria due to her investigator contribution in clinical trials from Array Biopharma, MSD, Abbvie, Amgen, GlaxoSmithKline, AstraZeneca, Merck Sharp & Dohme, Bristol-Myers Squibb, Novartis, Boehringer Ingelheim, Hoffmann-La Roche, Medimmune, Pierre-Fabre and Sanofi Aventis. F.P. received honoraria from Amgen, Merck Serono, Lilly, Sanofi, Bayer, Servier, MSD, AstraZeneca and Organon and research grants from AstraZeneca and BMS. G.K. is an employee of Novartis. G.V. has received a speaker's fee from MSD and Pierre Fabre and has held an advisory role with AstraZeneca. J.R. declares receiving honoraria from Sanofi and travel and accommodation expenses from Amgen, Merck and Sanofi. J.T. reports having a personal financial interest in the form of a scientific consultancy role for Array Biopharma, AstraZeneca, Avvinity, Bayer, Boehringer Ingelheim, Chugai, Daiichi Sankyo, F. Hoffmann-La Roche, Genentech, HalioDX, Hutchison MediPharma International, Ikena Oncology, Inspirna, IQVIA, Lilly, Menarini, Merck Serono, Merus, MSD, Mirati, Neophore, Novartis, Ona Therapeutics, Orion Biotechnology, Peptomyc, Pfizer, Pierre Fabre, Samsung Bioepis, Sanofi, Seattle Genetics, Scandion Oncology, Servier, Sotio Biotech, Taiho, Tessa Therapeutics and TheraMyc, as well as educational collaboration with Immedex, Medscape Education, MJH Life Sciences, PeerView Institute for Medical Education and Physicians Education Resource (PER). P.N. reports receiving honoraria or consultation fees from Novartis, Bayer and MSD Oncology and had travel and accommodation paid for or reimbursed by Novartis. R.A.T. reports receiving a research grant related to this study from Novartis and research grants unrelated to this study from AstraZeneca and Beigene. R.D. declares an advisory role for Roche and Boehringer Ingelheim and received a speaker's fee from Roche, Boehringer Ingelheim, Ipsen, Amgen, Servier, Sanofi, Libbs and Merck Sharp & Dohme and research grants from Merck and Pierre Fabre. R.P.-L. has acted in a consulting or advisory role for Roche, and she has participated in speaker bureaus sponsored by Roche and Pfizer. She is also the principal investigator in research grants to VHIO funded by AstraZeneca and Roche. S. Lonardi declares no conflict of interest inside the scope of the present work but declares interests in other projects from a consulting or advisory role (Amgen, Merck Serono, Lilly, AstraZeneca, Incyte, Daiichi-Sankyo, Bristol-Myers Squibb, Servier and MSD); speaker's bureau compensation from Roche, Lilly, Bristol-Myers Squibb, Servier, Merck Serono, Pierre-Fabre, GSK and Amgen; and research funding from Amgen, Merck Serono, Bayer, Roche, Lilly, AstraZeneca and Bristol-Myers Squibb. The other authors declare no conflicts of interest.

Additional information

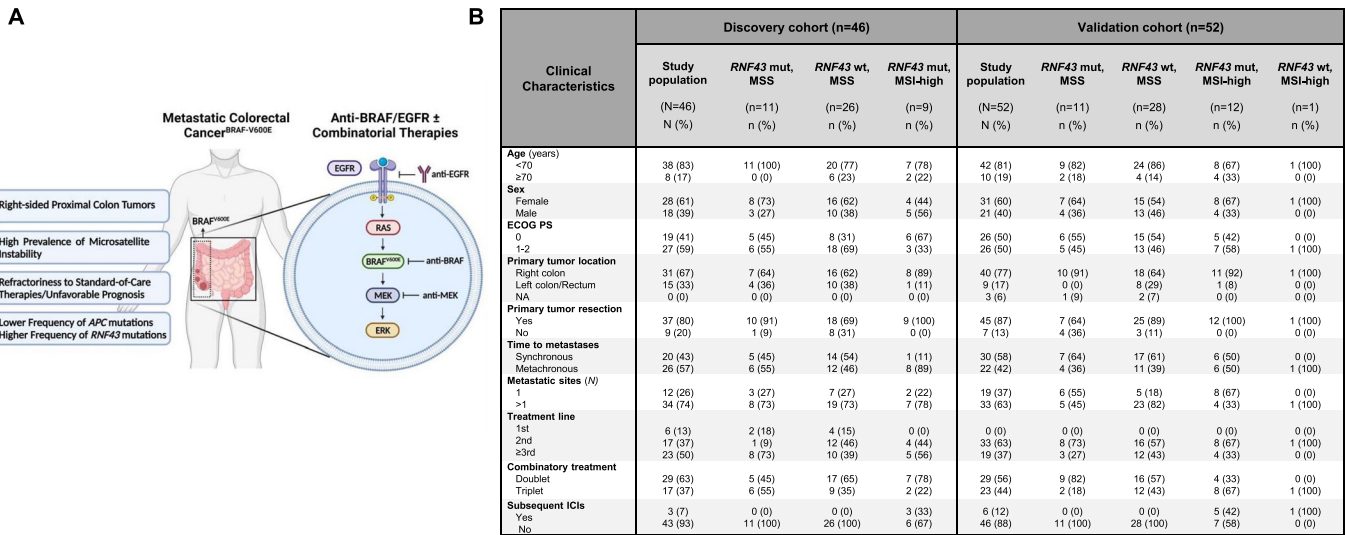
Extended data is available for this paper at <https://doi.org/10.1038/s41591-022-01976-z>.

Supplementary information The online version contains supplementary material available at <https://doi.org/10.1038/s41591-022-01976-z>.

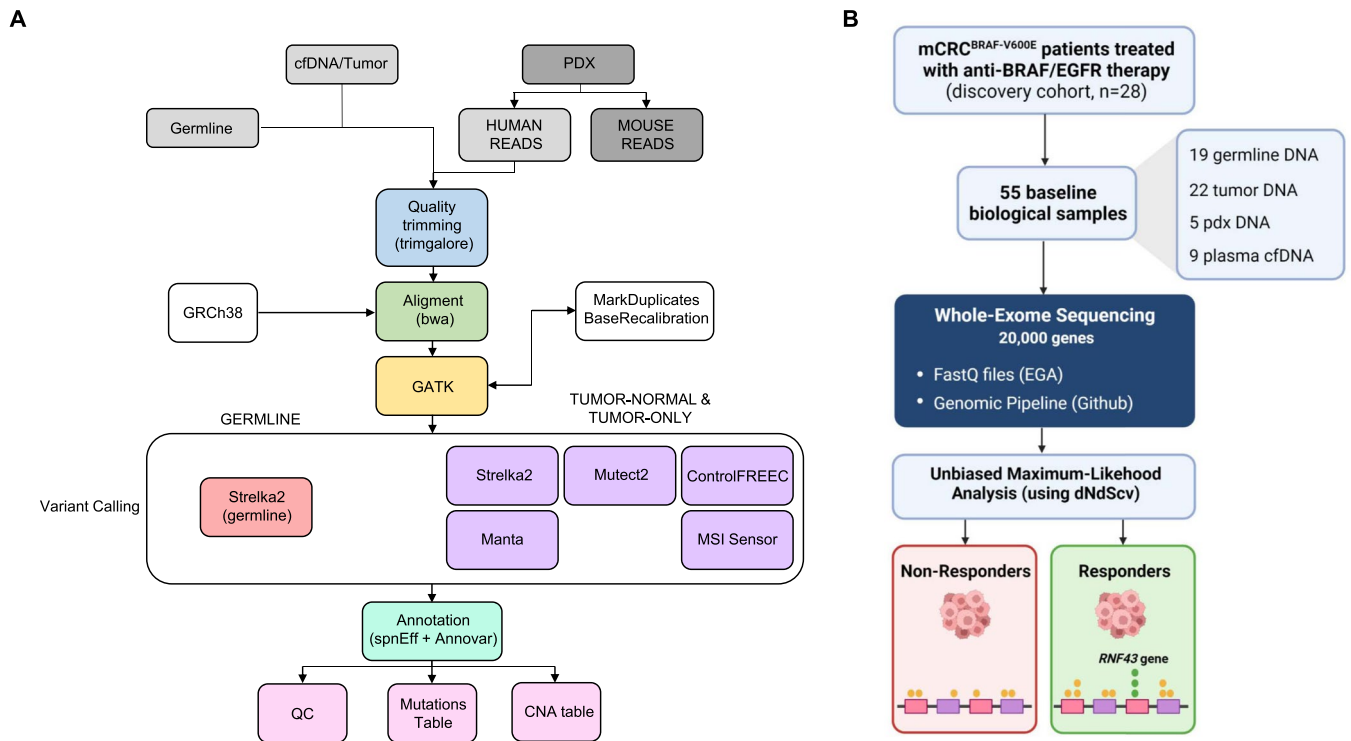
Correspondence and requests for materials should be addressed to Elena Elez or Rodrigo A. Toledo.

Peer review information *Nature Medicine* thanks Jan Paul Medema, Fortunato Ciardiello and Dominik Modest for their contribution to the peer review of this work. Primary Handling Editor: Joao Monteiro, in collaboration with the *Nature Medicine* team.

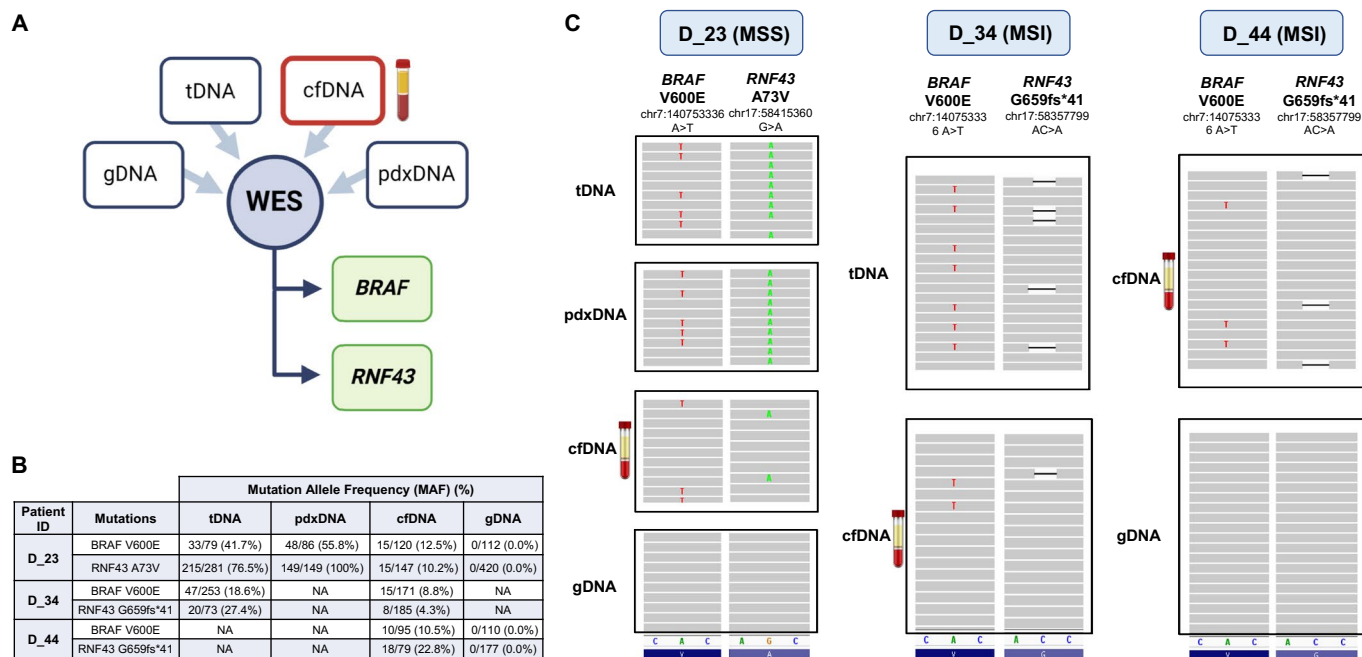
Reprints and permissions information is available at www.nature.com/reprints.



Extended Data Fig. 1 | Patients' characteristics. A) Patient and therapy flowchart. Specific clinical and genetic characteristics of mCRC^{BRAF-V600E} compared to mCRC^{BRAF-wild-type} tumors. Schematic description of the anti-BRAF/EGFR combinatorial therapies (doublet vs triplet) for patients with mCRC^{BRAF-V600E}. **B)** Clinical characteristics of patients in the discovery (n = 46) and validation (n = 52) cohorts. Abbreviations: ECOG PS, Eastern Cooperative Oncology Group Performance Status; ICIs, immune checkpoint inhibitors; MSI-high, microsatellite instability high; MSS, microsatellite stable.

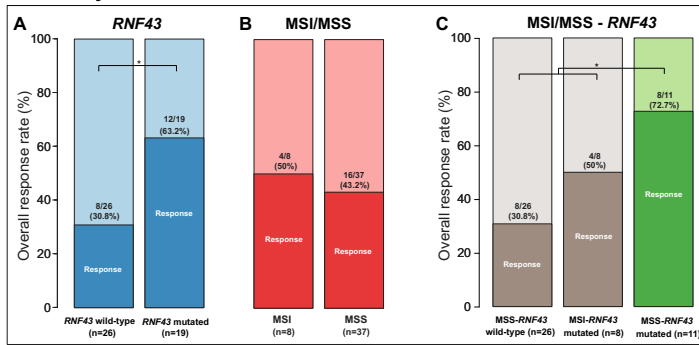


Extended Data Fig. 2 | Bioinformatics pipeline for genomic data analysis. A) Description of the Sarek bioinformatics pipeline, a Nextflow-based pipeline that integrates all the processing, mapping, variant calling, and QC steps⁴⁰, used for the WES analysis. **B)** WES based on responders vs non-responders from the discovery cohort ($n = 28$) followed by dNdScv²⁵ maximum-likelihood unbiased mutation enrichment analysis was used as the genomic biomarker discovery strategy on 55 biological samples from mCRC^{BRAF-V600E} patients collected at baseline to anti-BRAF/EGFR \pm MEKi therapies. The FastQ files have been deposited in the European Genome-phenome Archive (EGA, <https://ega-archive.org>) biorepository. The code of the bioinformatics pipelines can be found at <https://github.com/nf-core/sarek> and at <https://github.com/jfnararro/scitron>. Abbreviations: cfDNA, cell-free DNA; CNA, copy number alteration; QC, quality control; PDX, patient-derived xenograft.

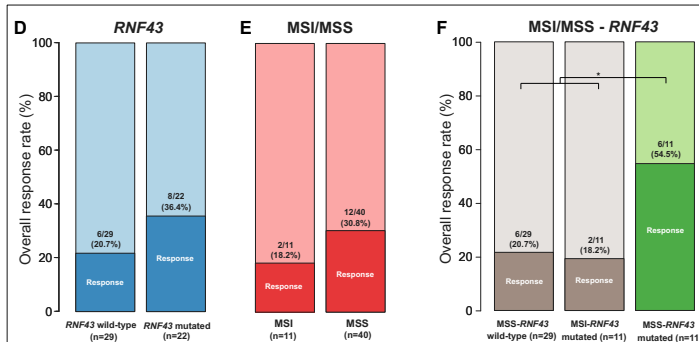


Extended Data Fig. 3 | The utility of liquid biopsy to assess *BRAF* and *RNF43* mutational status in patients with mCRC^{BRAF-V600E} treated with anti-BRAF/EGFR combinatorial therapies. **A)** WES was performed in 55 baseline biological samples from 19 gDNA, 22 tDNA, 9 cfDNA, and 5 pdxDNA from 28 patients with mCRC^{BRAF-V600E} from the discovery cohort treated with anti-BRAF/EGFR combinatorial therapies. The presence of the *BRAF*^{V600E} and *RNF43* mutations was interrogated in tumor-derived and plasma-derived samples. **B)** Mutation allele frequencies (MAF) of the *BRAF* and *RNF43* specific mutations are shown to gDNA, tDNA, and pdxDNA from patients with multiple samples which are available. **C)** *BRAF*^{V600E} and *RNF43* mutations were detected not only in tDNA and/or pdxDNA but also in available cfDNA samples, suggesting the utility of liquid biopsy for the assessment of these biomarkers. Abbreviations: gDNA, germline DNA; tDNA, tumor DNA; cfDNA, cell-free DNA; MSI, microsatellite instability high; MSS, microsatellite stable; pdxDNA, patient-derived xenograft DNA.

Discovery cohort



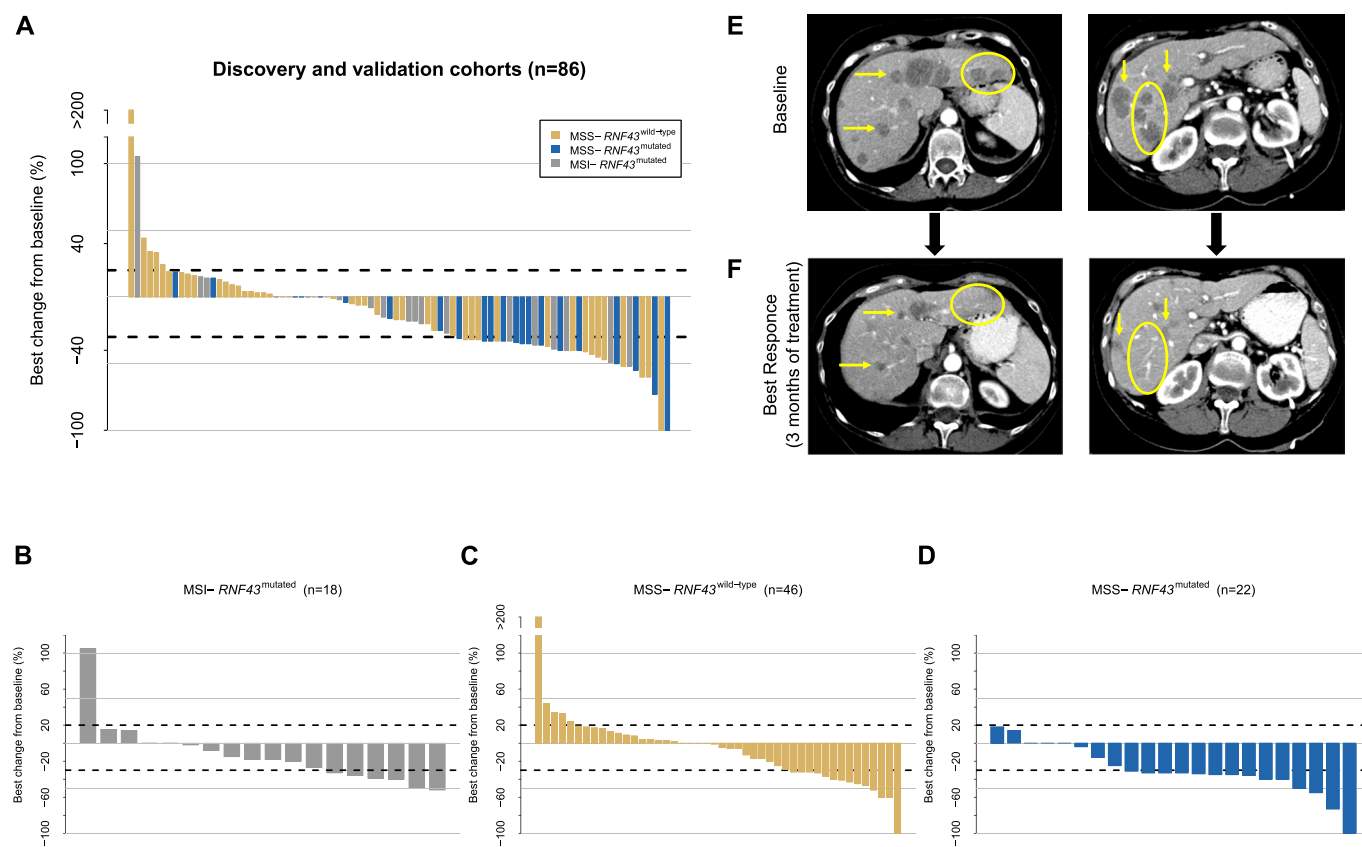
Validation cohort



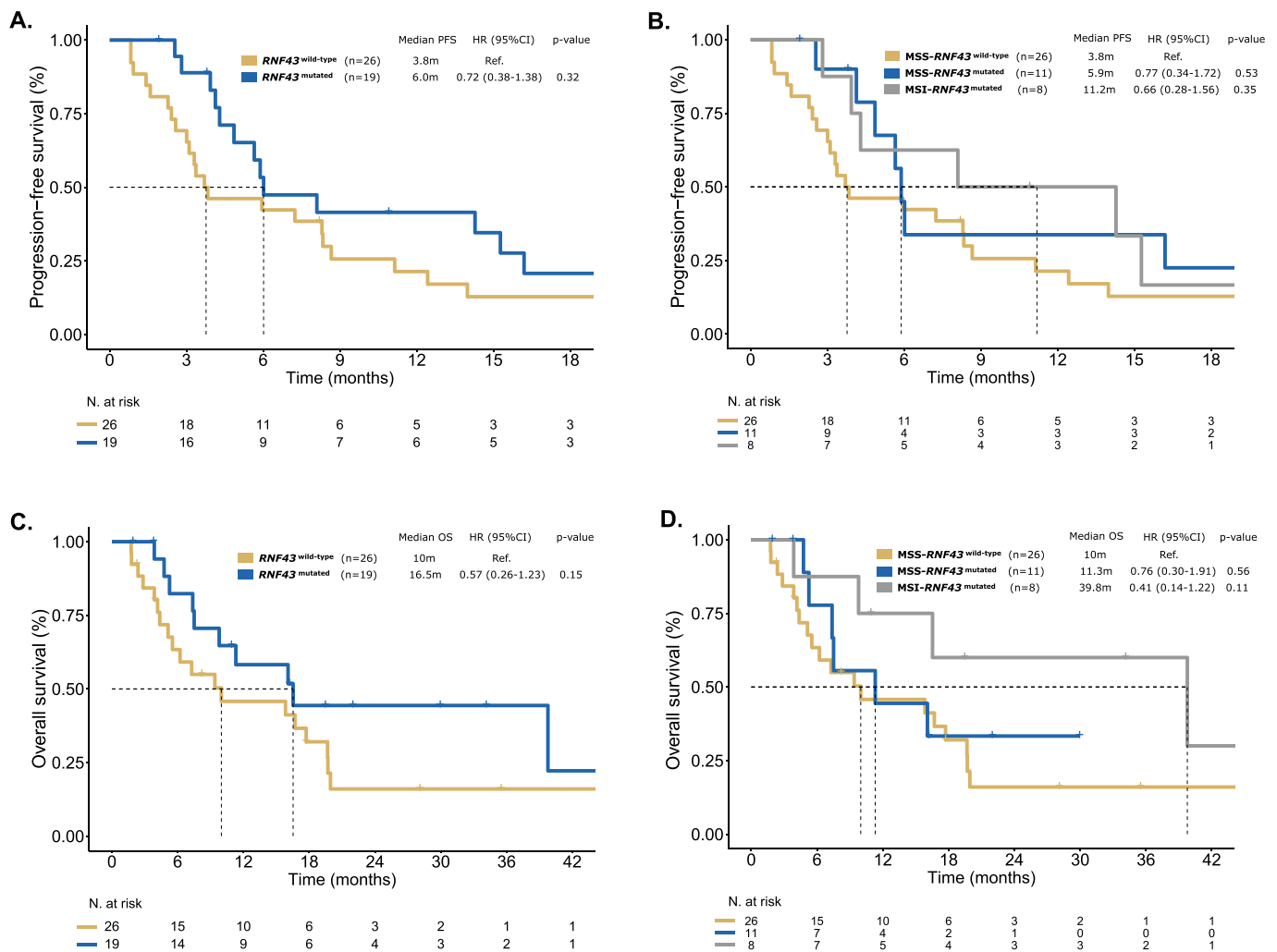
G

	Discovery cohort (n=45)			Validation cohort (n=50)
	RNF43 mutation	MSS/MSI status	RNF43 mutation / MSS status	RNF43 mutation / MSS/MSI status
Sensitivity (%)	60.0	80.0	40.0	42.9
Specificity (%)	72.0	16.0	88.0	86.5
PPV (%)	63.2	43.2	72.7	54.6
NPV (%)	69.2	50.0	64.7	80.0
Accuracy	66.7	44.4	66.7	74.5

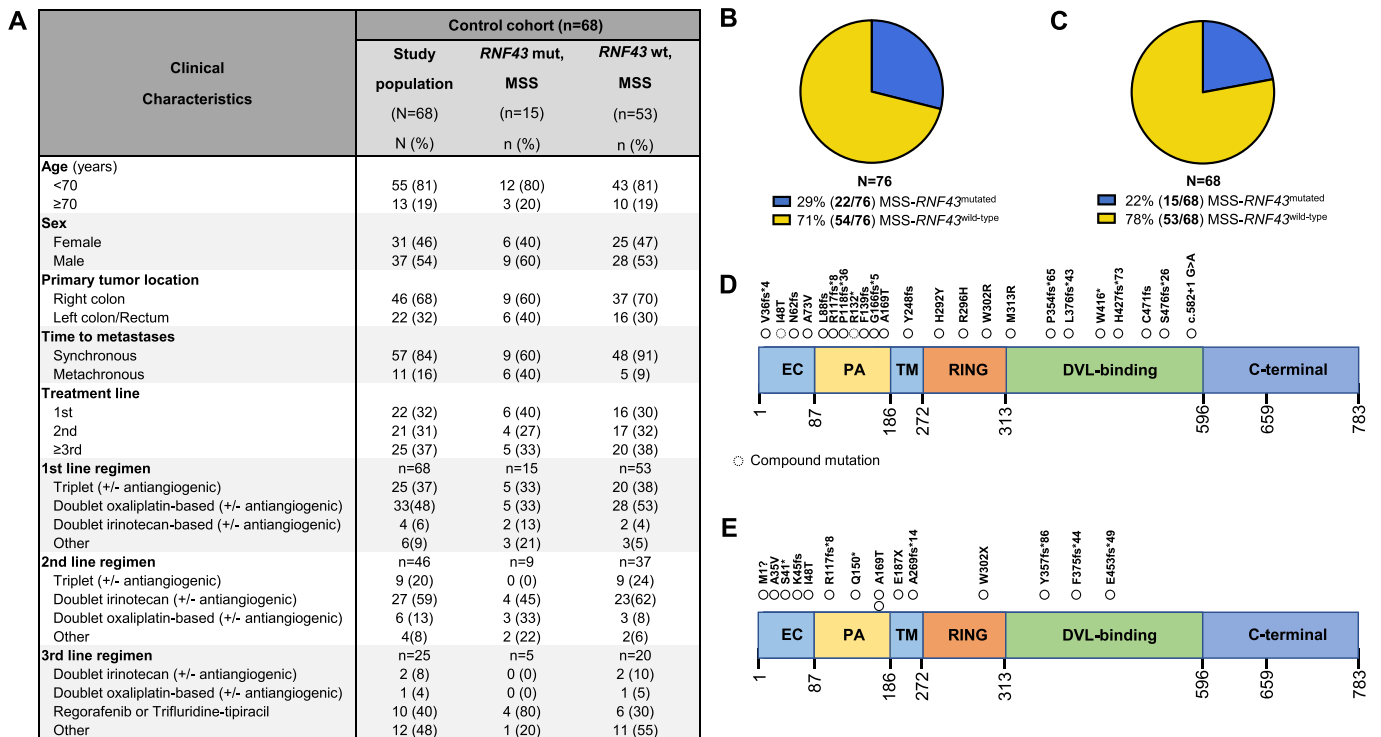
Extended Data Fig. 4 | Overall response rate (ORR) (%) of the discovery (n = 45, A–C) and validation (n = 50, D–F) cohorts and diagnostic performance analyses (G) defined by MSS/MSI and RNF43 mutation statuses. **A**) Patients with *RNF43*^{mutated} tumors exhibited an increased ORR (63%) compared to patients with *RNF43*^{wild-type} (31%). **B**) There were no significant differences between ORRs according to MSI/MSS status (50% and 43%, respectively). **C**) Interestingly, patients with mCRC^{BRAF-V600E} with MSS-*RNF43*^{mutated} tumors demonstrated increased ORR (73%) compared to the other groups, as MSI-*RNF43*^{mutated} and MSS-*RNF43*^{wild-type} (50% and 31%, respectively) ($P = 0.03$). Chi-square test was used for the statistical analysis. **D–F**) ORR of the validation cohort including 50 patients with mCRC^{BRAF-V600E} tumors treated with anti-BRAF/EGFR combinatorial therapies in 2nd or 3rd line. **D**) *RNF43*^{mutated} group exhibited an increased ORR (36%) compared to *RNF43*^{wild-type} group (21%). **E**) There were no significant differences between MSI/MSS status (31% and 17%, respectively). **F**) Interestingly, MSS-*RNF43*^{mutated} group showed increased ORR (54%) compared to the other groups, MSI-*RNF43*^{mutated} and MSS-*RNF43*^{wild-type} (18% and 21%), respectively ($P = 0.02$). Chi-square test was used for the statistical analysis ($*P < 0.05$). **G**) Table showing results of the accuracy, sensitivity, specificity, and positive (PPV) and negative predictive value (NPV) calculated to quantify the diagnostic performance of statuses of each potential biomarker (MSS/MSI and *RNF43* separated, and MSS/MSI-*RNF43* combined, in the discovery and validation cohorts). Abbreviations: MSI, microsatellite instability high; MSS, microsatellite stable.



Extended Data Fig. 5 | Waterfall plots depicting different molecular subtypes. **A)** Integrated waterfall plot showing best change in the total diameter of target lesions from baseline in 86 patients with mCRC^{BRAF-V600E} tumors treated with anti-BRAF/EGFR combinatory therapies (discovery cohort, n = 44, plus validation cohort, n = 42). As a common in real-world clinical practice for aggressive tumors like mCRC^{BRAF-V600E}, images from a proportion of patients (n = 12) were not available, mostly due to rapid clinical deterioration. **B-D)** Waterfall plots including patients with the different molecular subtypes: **B)** MSI-*RNF43*^{mutated} tumors are shown in gray, **C)** MSS-*RNF43*^{wild-type} tumors are shown in yellow, and **D)** MSS-*RNF43*^{mutated} tumors are shown in blue. **E)** The post-contrast CT scan at baseline shows multiple liver metastases (yellow arrows) in a patient with mCRC^{BRAF-V600E} with a MSS-*RNF43*^{mutated} tumor. **F)** The post-contrast CT scan after 3 months of treatment shows marked reduction in size of the liver metastases (yellow arrows); some of the lesions are no longer seen in the follow-up CT-scan (yellow circles). Abbreviations: MSI, microsatellite instability high; MSS, microsatellite stable.

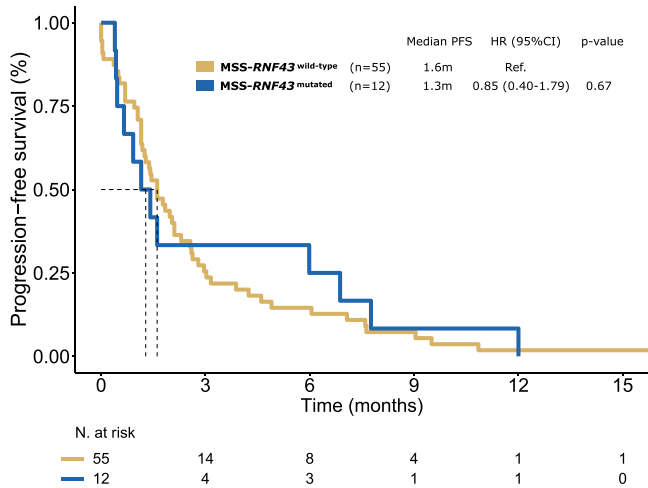


Extended Data Fig. 6 | Kaplan-Meier curves of PFS and OS from patients with mCRC^{BRAF-V600E} tumors (discovery cohort, n = 45) treated with anti-BRAF/EGFR combinatory therapies with regard to *RNF43* mutations (left) and *RNF43* mutations combined with MSS/MSI status (right). **A) PFS of patients with *RNF43*^{mutated} (n = 19) and *RNF43*^{wild-type} (n = 26) tumors and **B)** combined *RNF43* and MSS/MSI statuses (MSS-*RNF43*^{wild-type} [n = 26], MSS-*RNF43*^{mutated} [n = 11], MSI-*RNF43*^{mutated} [n = 8]). **C)** Event-free survival of patients with *RNF43*^{mutated} (n = 19) and *RNF43*^{wild-type} (n = 26) tumors and **D)** combined *RNF43* and MSS/MSI statuses (MSS-*RNF43*^{wild-type} [n = 26], MSS-*RNF43*^{mutated} [n = 11], MSI-*RNF43*^{mutated} [n = 8]). Cox models were used to obtain hazard ratios with 95% CIs, and the two-sided log-rank test was used for statistical comparisons without adjustment for multiplicity. Colors indicate molecular subtypes: *RNF43*^{wild-type} tumors with or without MSS (yellow), *RNF43*^{mutated} tumors with or without MSS (blue) and MSI-*RNF43*^{mutated} tumors (gray). Significant values are shown in bold. Abbreviations: CI, confidence interval; HR, hazard ratio.**

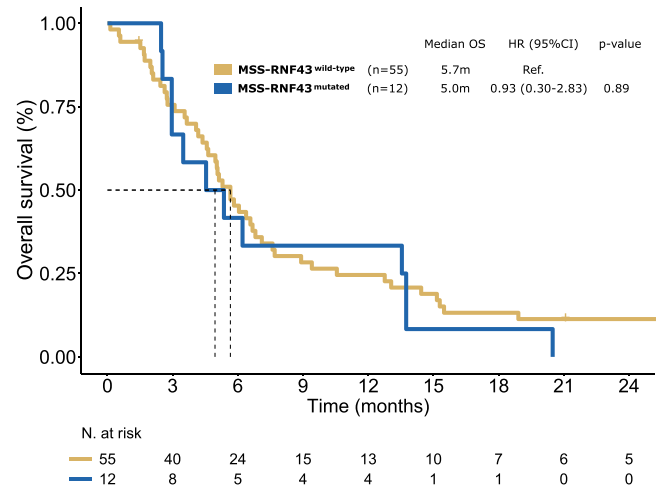


Extended Data Fig. 7 | Clinical characteristics and mutational profile of patients with mCRC^{BRAF-V600E} treated with no anti-BRAF/EGFR combinatorial therapies. A Clinical and therapeutic characteristics of patients from the control cohort, patients receiving standard chemotherapy ± antiangiogenic agents (total N = 68). These patients received in total 135 chemotherapy regimens with/without anti-angiogenic drugs during first, second, or third lines. A total of 67 treatment lines (second and third line) in MSS patients were analyzed. **B-E** Comparison of *RNF43* mutation frequencies and protein location between discovery/validation (**B,D**) and control (**C,E**) cohorts. *RNF43* mutation frequencies of the mCRC^{BRAF-V600E} MSS subgroup from discovery/validation (29%, 22/76) and control (22%, 15/68) cohorts were similar (**B, C**), respectively. Also, the MSS discovery/validation and control cohorts showed a similar *RNF43* mutational profile regarding localization and predictive functional status (**D, E**). Abbreviations: MSS, microsatellite stable.

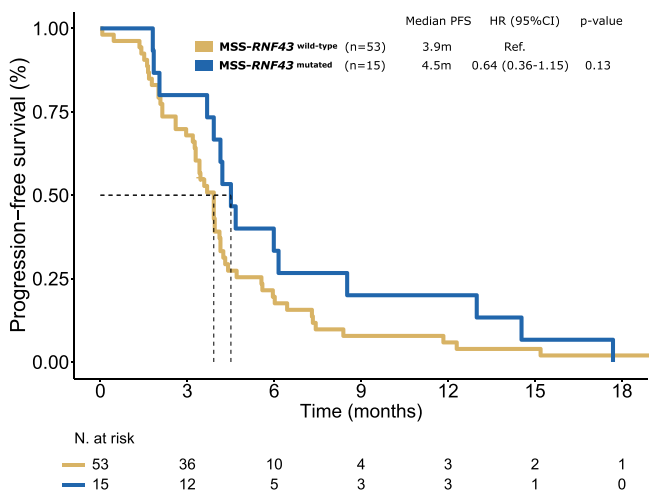
A. PFS in MSS patients treated in 2L and 3L



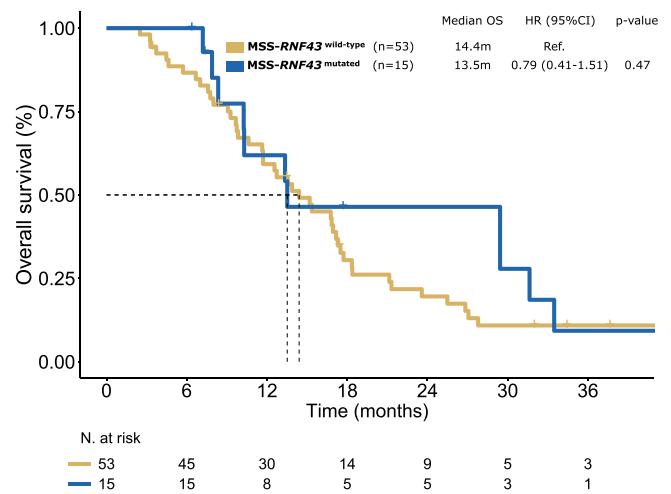
B. OS in MSS patients treated in 2L and 3L



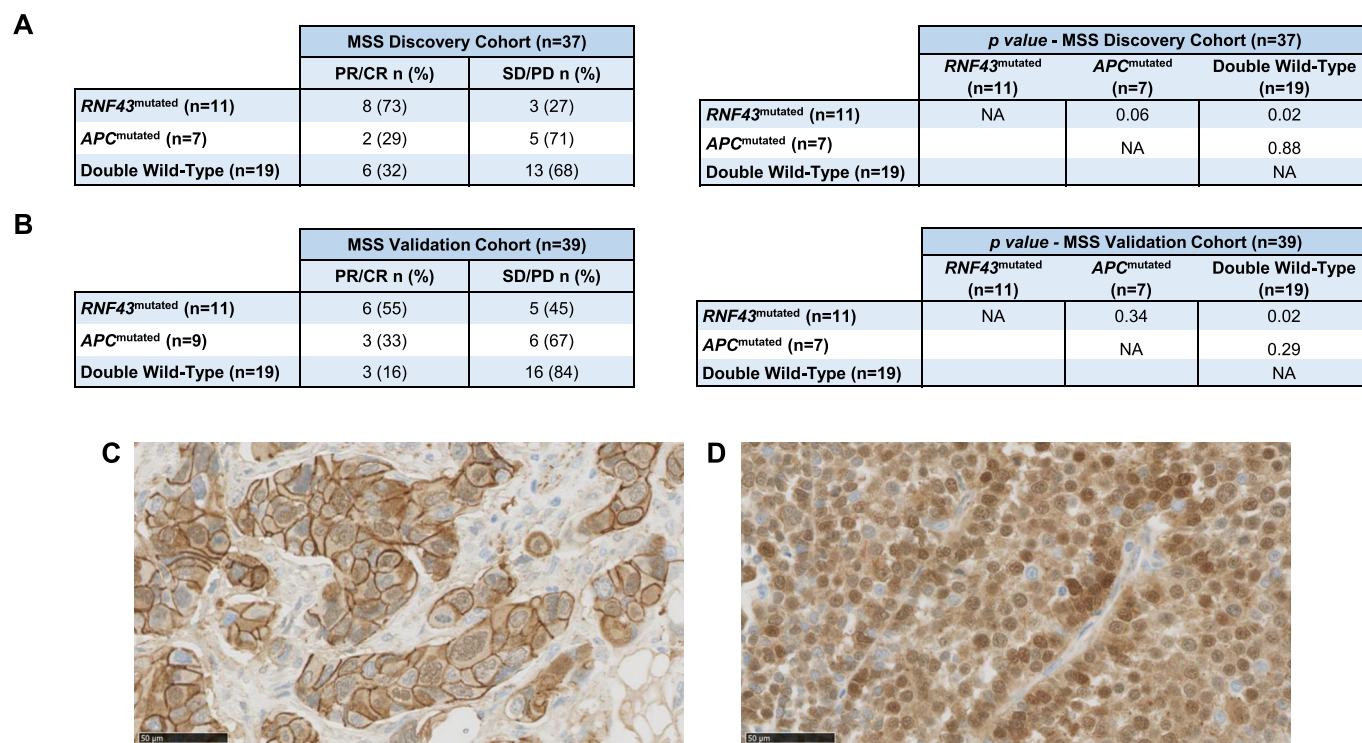
C. PFS in MSS patients treated in 1L



D. OS in MSS patients treated in 1L



Extended Data Fig. 8 | Analysis of the prognostic/predictive value of *RNF43* mutations in the control cohort of patients with mCRC^{BRAF-V600E} with MSS tumors treated with standard-of-care regimens only, with no exposure to anti-BRAF therapies. A, B) Kaplan-Meier curves of PFS and OS from the control cohort treated in second or third line (n = 67) C, D) and in first line (n = 68) with standard-of-care regimens only, with no exposure to anti-BRAF therapies. Colors refer to molecular subtypes: *RNF43*^{wild-type} (yellow), *RNF43*^{mutated} tumors (blue)^{wild-type}. Cox models were used to obtain hazard ratios with 95% CI, and the two-sided log-rank test was used for statistical comparisons without adjustment for multiplicity. Abbreviations: CI, confidence interval; HR, hazard ratio.



Extended Data Fig. 9 | Mutation frequencies of *RNF43* and *APC* genes in MSS status and immunohistochemical analysis against human β -catenin of mCRC^{BRAF-V600E} tumor samples. **A, B Mutation frequencies of *RNF43* and *APC* genes, and response status from patients with mCRC^{BRAF-V600E} with MSS tumors from the discovery (**A**) and validation (**B**) cohorts. Chi-square test was used for the statistical analysis. Abbreviations: CR, complete response; MSS, microsatellite stable; PD, progressive disease; PR, partial response; SD, stable disease. **C–D** Immunohistochemical analysis against human β -catenin was performed in MSS-*RNF43*^{wild-type}, MSS-*RNF43*^{mutated}, and MSI-*RNF43*^{mutated} mCRC^{BRAF-V600E} tumor samples (n = 33) to search for potential differential pattern in total expression or cellular localization of β -catenin protein. No correlation was found between β -catenin protein expression levels (0, no staining; 1, weak; 2, moderate; and 3, strong) and cellular localization (cytoplasm, membrane, nucleus) with response to anti-BRAF/EGFR \pm combinatorial therapies. Representative immunohistochemistry for β -catenin with strong membrane positivity, weak-moderate cytoplasmic positivity, and few weak nucleus positivity (magnification 40x) (**C**) and strong-moderate nuclear and cytoplasmic positivity (**D**) (magnification 40x).**

Reporting Summary

Nature Portfolio wishes to improve the reproducibility of the work that we publish. This form provides structure for consistency and transparency in reporting. For further information on Nature Portfolio policies, see our [Editorial Policies](#) and the [Editorial Policy Checklist](#).

Statistics

For all statistical analyses, confirm that the following items are present in the figure legend, table legend, main text, or Methods section.

n/a Confirmed

- | | | |
|-------------------------------------|-------------------------------------|--|
| <input type="checkbox"/> | <input checked="" type="checkbox"/> | The exact sample size (n) for each experimental group/condition, given as a discrete number and unit of measurement |
| <input type="checkbox"/> | <input checked="" type="checkbox"/> | A statement on whether measurements were taken from distinct samples or whether the same sample was measured repeatedly |
| <input type="checkbox"/> | <input checked="" type="checkbox"/> | The statistical test(s) used AND whether they are one- or two-sided
<i>Only common tests should be described solely by name; describe more complex techniques in the Methods section.</i> |
| <input type="checkbox"/> | <input checked="" type="checkbox"/> | A description of all covariates tested |
| <input type="checkbox"/> | <input checked="" type="checkbox"/> | A description of any assumptions or corrections, such as tests of normality and adjustment for multiple comparisons |
| <input type="checkbox"/> | <input checked="" type="checkbox"/> | A full description of the statistical parameters including central tendency (e.g. means) or other basic estimates (e.g. regression coefficient) AND variation (e.g. standard deviation) or associated estimates of uncertainty (e.g. confidence intervals) |
| <input type="checkbox"/> | <input checked="" type="checkbox"/> | For null hypothesis testing, the test statistic (e.g. F , t , r) with confidence intervals, effect sizes, degrees of freedom and P value noted
<i>Give P values as exact values whenever suitable.</i> |
| <input checked="" type="checkbox"/> | <input type="checkbox"/> | For Bayesian analysis, information on the choice of priors and Markov chain Monte Carlo settings |
| <input checked="" type="checkbox"/> | <input type="checkbox"/> | For hierarchical and complex designs, identification of the appropriate level for tests and full reporting of outcomes |
| <input checked="" type="checkbox"/> | <input type="checkbox"/> | Estimates of effect sizes (e.g. Cohen's d , Pearson's r), indicating how they were calculated |

Our web collection on [statistics for biologists](#) contains articles on many of the points above.

Software and code

Policy information about [availability of computer code](#)

Data collection No software was used for data collection.

Data analysis The code of the pipeline that was used to process all the samples can be found at <https://github.com/nf-core/sarek>. Sarek is a Nextflow based pipeline that integrates all the processing, mapping, variant calling, and QC steps. The code used for post-processing, filtering, validation, and analysis of the mutational data is available at <https://github.com/jfnavarro/scitron>. All statistical analyses were performed using R statistical software version 4.1.2.

For manuscripts utilizing custom algorithms or software that are central to the research but not yet described in published literature, software must be made available to editors and reviewers. We strongly encourage code deposition in a community repository (e.g. GitHub). See the Nature Portfolio [guidelines for submitting code & software](#) for further information.

Data

Policy information about [availability of data](#)

All manuscripts must include a [data availability statement](#). This statement should provide the following information, where applicable:

- Accession codes, unique identifiers, or web links for publicly available datasets
- A description of any restrictions on data availability
- For clinical datasets or third party data, please ensure that the statement adheres to our [policy](#)

Reference genome GRCh38 was used for the alignment. The FastQ files corresponding to the whole exome-sequencing (WES) data from clinical samples analyzed in the paper have been deposited in the European Genome-phenome Archive (EGA, <https://ega-archive.org>) biorepository under the ID dataset of Study ID: EGAS00001006247 and the Dataset ID: EGAD00001008755 with appropriate measures for controlled access (collaboration required (DUO: 0000020), ethics

Field-specific reporting

Please select the one below that is the best fit for your research. If you are not sure, read the appropriate sections before making your selection.

- Life sciences Behavioural & social sciences Ecological, evolutionary & environmental sciences

For a reference copy of the document with all sections, see nature.com/documents/nr-reporting-summary-flat.pdf

Life sciences study design

All studies must disclose on these points even when the disclosure is negative.

Sample size	Not pre-specific sample size calculation was performed for this project. The study included all available mCRC BRAF-V600E patients with information in RNF43 gene. A total of 166 metastatic mCRC BRAF-V600E patients (98 treated with anti-BRAF/EGFR therapies and 68 treated with standard-of-care not including BRAFi therapies) were included in the current study. Of the treated with anti-BRAF/EGFR therapies, the discovery cohort was composed of 46 patients from the Vall d'Hebron University Hospital (Barcelona, Spain) prospectively included from 2013 to 2021, and the validation cohort comprised 52 patients from three academic hospitals from Italy (Fondazione IRCCS Istituto Nazionale dei Tumori, Milan, Italy; Azienda Ospedaliero-Universitaria Pisana, University Hospital of Pisa, Pisa, Italy; Istituto Oncologico Veneto IOV-IRCCS, Padova, Italy). Control cohort was composed by patients from all the above referred institutes. The validation cohort (n=52) had > 80% power to validate statistically and clinically significant differences in PFS and OS with hazard ratio of 0.45 or lower using two-sided 0.05 alpha error.
Data exclusions	No genomics data were excluded from the analyses. One patient from the discovery cohort and another from the validation cohort were not evaluable for response and were excluded from the overall response rate (ORR) analysis.
Replication	The results obtained in the discovery cohort were confirmed in an external validation cohort.
Randomization	This was a retrospective study and no randomization was performed. The current study aims to explore the predictive value of RNF43 status (baseline characteristic) but not the efficacy of a specific treatment strategy. In this particular scenario, randomization is not strictly needed to generate the set of evidence.
Blinding	Blindness is not relevant to studies searching for potential biomarkers of response to anti-cancer therapies. Importantly, an unbiased positive selection analysis was applied using mutation data obtained from whole-exome sequencing (WES) of the tumors from the responders and non responders. Specifically, the unbiased maximum-likelihood analysis of WES mutational data from responders vs non-responders using dNdScv identified the RNF43 gene as a top candidate gene associated with ORR (p- and q-values <0.001).

Reporting for specific materials, systems and methods

We require information from authors about some types of materials, experimental systems and methods used in many studies. Here, indicate whether each material, system or method listed is relevant to your study. If you are not sure if a list item applies to your research, read the appropriate section before selecting a response.

Materials & experimental systems

n/a	Involved in the study
<input type="checkbox"/>	<input checked="" type="checkbox"/> Antibodies
<input type="checkbox"/>	<input checked="" type="checkbox"/> Eukaryotic cell lines
<input checked="" type="checkbox"/>	<input type="checkbox"/> Palaeontology and archaeology
<input checked="" type="checkbox"/>	<input type="checkbox"/> Animals and other organisms
<input type="checkbox"/>	<input checked="" type="checkbox"/> Human research participants
<input type="checkbox"/>	<input checked="" type="checkbox"/> Clinical data
<input checked="" type="checkbox"/>	<input type="checkbox"/> Dual use research of concern

Methods

n/a	Involved in the study
<input checked="" type="checkbox"/>	<input type="checkbox"/> ChIP-seq
<input checked="" type="checkbox"/>	<input type="checkbox"/> Flow cytometry
<input checked="" type="checkbox"/>	<input type="checkbox"/> MRI-based neuroimaging

Antibodies

Antibodies used	Anti-FLAG Antibody (1:1000, cat.# F1804, Sigma-Aldrich, St. Louis, MO, USA); Mouse anti- β -actin (1:1000, cat.# sc-47778, Santa Cruz, CA, USA); IRDye 680 goat anti-mouse (1:10.000, cat.# LI 926-68070, LI-COR Biosciences, Lincoln, NE, USA); human β -catenin Antibody (prediluted, cat.# 760-4242, lot V0002678, Beta-Catenin Mouse Monoclonal Antibody, clone 14, Cell Marque, Rocklin, CA, USA); Ventana UltraView Universal DAB Detection Kit (cat.#. 760-500, Roche, Penzberg, Germany).
Validation	Anti-FLAG antibody (https://scholar.google.com/scholar?hl=en&as_sdt=0%2C5&as_vis=1&q=f1804+Flag+sigma&btnG=); Mouse anti- β -actin (https://www.scdb.com/es/p/beta-actin-antibody-c4); IRDye 680 goat anti-mouse (https://scholar.google.com/scholar?hl=en&as_sdt=0%2C5&as_vis=1&q=IRDye+680+goat+anti-mouse+LI+926-68070&btnG=); betacatenin mouse monoclonal antibody

Eukaryotic cell lines

Policy information about [cell lines](#)

Cell line source(s)	HEK293T has been cultured in the Erasmus MC-University Medical Center, Rotterdam, the Netherlands for decades and no specific origin is reported.
Authentication	Identity of HEK293T cell line was confirmed by the Erasmus Molecular Diagnostics Department, using Powerplex-16 STR genotyping (Promega, Leiden, The Netherlands).
Mycoplasma contamination	The HEK293T cell line tested negative for mycoplasma based on the real-time PCR method at Eurofins GATC-Biotech (Konstanz, Germany).
Commonly misidentified lines (See ICLAC register)	None

Human research participants

Policy information about [studies involving human research participants](#)

Population characteristics	A total of 166 patients with metastatic CRC-BRAF-V600E patients were included in the current study. 98 patients were treated with anti-BRAF/EGFR therapies: 46 patients belonged to the discovery cohort: female, 28/46 (61%) and male, 18/46 (39%) and the median age at diagnosis was 61 years old (range: 33-82) and 52 patients belonged to the validation cohort: female, 31/52 (60%) and male 21/52 (40%) and the median age at diagnosis was 62 years old (range: 38-80). Moreover, 68 patients were treated with non-BRAFi standard-of-care therapies (control cohort): female, 31/68 (46%) and male, 37/68 (54%) and median age at diagnosis 60.5 years old (range: 30-80).
Recruitment	Clinical data and samples from BRAF-V600E-mutated mCRC patients from the Vall d'Hebron Institute of Oncology (VHIO), Barcelona, Spain; Veneto Institute of Oncology IRCCS, Padova, Italy; Azienda Ospedaliero-Universitaria Pisana, University of Pisa, Pisa, Italy and Fondazione IRCCS Istituto Nazionale dei Tumori, Milan, Italy were retrospectively obtained and included in the study. There was no relevant bias on the inclusion of these patients that could affect the further analyses.
Ethics oversight	The study was approved by each investigational site's institutional review board/ethics committee: Vall d'Hebron Institute of Oncology (VHIO), Barcelona, Spain; Veneto Institute of Oncology IRCCS, Padova, Italy; Azienda Ospedaliero-Universitaria Pisana, University of Pisa, Pisa, Italy and Fondazione IRCCS Istituto Nazionale dei Tumori, Milan, Italy. The research was conducted in accordance with the Declaration of Helsinki and local data protection laws. All patients provided written informed consent before enrollment. All data provided are anonymized in line with applicable laws and regulations.

Note that full information on the approval of the study protocol must also be provided in the manuscript.

Clinical data

Policy information about [clinical studies](#)

All manuscripts should comply with the ICMJE [guidelines for publication of clinical research](#) and a completed [CONSORT checklist](#) must be included with all submissions.

Clinical trial registration	This was a translational research study, not a formal clinical trial.
Study protocol	This was a translational research study, not a formal clinical trial.
Data collection	Patients, genetics and clinical information from each center were retrospectively collected and data integrated for the study.
Outcomes	The evaluable outcomes were overall response rates (ORR), progression-free survival (PFS), and overall survival (OS).